Materials Sciences Corporation

DRAFT

STRESS ANALYSIS AND DAMAGE MODELING OF TEXTILE COMPOSITES

Technical Final Report

MSC TFR 3909/DA09

August, 1999

Contract No. F49620-96-C-0018

Principal Investigator: Gerry V. Flanagan

Technical Monitor: Ozden Ochoa

Prepared For:

Air Force Office of Scientific Research
110 Duncan Avenue, Suite B 115
Bolling AFB, DC 20332-0001

Suite 250, 500 Office Center Drive
Fort Washington, PA 19034
Tel: 215-542-8400 Fax: 215-542-8401

25 Years Advanced Composites Technology

AFRL-SR-BL-TR-99-

0230

REPORT DOCUMENTATION PAGE

1. AGENCY USE ONLY (*Leave blank*)	2. REPORT DATE	3. REPORT TYPE AND DATES COVERED
	August, 1999	Technical Final Report – 5/15/96 to 5/14/99

4. TITLE AND SUBTITLE

Stress Analysis and Damage Modeling of Textile Composites

5. FUNDING NUMBERS

F49620-96-C-0018

6. AUTHORS(S)

Manohar G. Kollegal, Ph.D., Sailendra N. Chatterjee, Ph.D., Gerry V. Flanagan

7. PERFORMING ORGANIZATION NAME(S) AND ADDRESS(ES)

Materials Sciences Corporation
500 Office Center Drive, Suite 250
Fort Washington, PA 19034

8. PERFORMING ORGANIZATION REPORT NUMBER

MSC TFR 3909/DA09

9. SPONSORING/MONITORING AGENCY NAME(S) AND ADDRESS(ES)

Prof. Ozden Ochoa
Air Force Office of Scientific Research
110 Duncan Avenue, Suite B115
Rolling AFB, DC 20332-8050

10. SPONSORING/MONITORING AGENCY REPORT NUMBER

11. SUPPLEMENTARY NOTES

12a. DISTRIBUTION/AVAILABILITY STATEMENT

Distribution Statement A: Approved for public release, distribution is unlimited.

12B. DISTRIBUTION CODE

13. ABSTRACT (*Maximum 200 words*)

Micromechanics of woven fabrics is studied using three dimensional finite elements which allow detailed modeling of the geometric complexities of the yarns and spatial material variations within the fabric. The undulation of the yarns combined with the varying cross-section profile of the yarn causes geometric nonlinear effects to influence the weave response. Material nonlinearity combined with high local stress fields can result in a variety of damage mechanisms such as matrix cracking, fiber breakage, and delamination which influence the overall properties of the composite. Damages in the composite constituents are modeled on a continuum basis and related to its material constitutive behavior. The 3D constitutive laws describing matrix and yarn behavior are developed using a damage mechanics based approach with the dissipated energy density as the damage parameter. The strain energy dissipation (SED) concept is employed to describe the damage state and current stiffnesses of the weave constituents. The constitutive laws for the materials are implemented through an user-defined subroutine and linked with the finite element analysis program, ABAQUS. A progressive failure analysis of plain woven fabrics subjected to tension and in-plane shear is performed considering both geometric and material nonlinearities. The initiation and progression of damage within the fabric is investigated and the significant damage mechanisms outlined.

14. SUBJECT TERMS
Textile composites, Micromechanics, Strain Energy Dissipation, Damage Mechanics, Constitutive Laws

15. NUMBER OF PAGES
81

16. PRICE CODE

17. SECURITY CLASSIFICATION OF REPORT	18. SECURITY CLASSIFICATION OF THIS PAGE	19. SECURITY CLASSIFICATION OF ABSTRACT	20. LIMITATION OF ABSTRACT
UNCLASSIFIED	UNCLASSIFIED	UNCLASSIFIED	Unlimited

NSN 7540-01-280-5500

Standard From 298 (rev. 2-89)
Prescribed by ANSI Std. Z39-18
298-102

TABLE OF CONTENTS

OBJECTIVE

The goals of this effort are:

- Select and develop methods for the analysis of the thermomechanical behavior of textile composite materials.
- Perform analysis of selected textile forms, including 2-D braids and weaves, and potentially 3-D architectures.
- Develop failure initiation and growth methodology for textile composites, including the growth and coalescence of internal cracking.
- Study the relationship of fabric architecture and failure sequence in a variety of textile composites.

SUMMARY OF ACCOMPLISHMENTS

To date, different analytical techniques were examined for their suitability for thermomechanical analysis of textile composites.

- The concept of equivalent homogeneity was used to derive relationships between average stresses and average strains within a fabric (see Appendix C). Representative volume elements (RVE) consisting of several non-homogeneous layers (fabric/matrix) were considered. Methods for calculating simple bounds on the effective properties of woven laminates were also suggested.
- Various numerical approaches for woven composites using *h*-element, *p*-element and novel meshing techniques were investigated (see Appendix D). Automated mesh generation codes were developed to rapidly create detailed FE models of typical two-dimensional textile forms. The mesh generation tools are modular and allow parametric modeling of the fabric geometry. The symmetry and antisymmetry of material distribution arising out of the repeating weave pattern can be used advantageously to reduce the problem size. This has been demonstrated in the case of plain woven fabrics. The models were analyzed using a commercial FEA code, ABAQUS, to compute their elastic properties and their mechanical response.

- Nonlinear material behavior and damage growth in textile composites was investigated using damage mechanics based constitutive laws. The strain energy dissipation was chosen as the damage parameter and used to describe a set of damage surfaces. Material models were developed for each of the weave constituents viz. yarn and pure matrix to describe their constitutive relationships and damage state. Interface subroutines were developed to link the developed material model codes with a general-purpose finite element analysis program.
- The developed damage modeling methodology is demonstrated for plain woven fabrics. Progressive failure analyses of some plain weave composites subjected to tension and in-plane shear are carried out. The different damage mechanisms causing failure of the fabric under on-axes and off-axes loading conditions are studied. Parametric studies to study the effect of yarn waviness and fiber volume fraction on the predicted elastic properties of plain weaves are also done.

INTRODUCTION

Micromechanics of textile composites has been the focus of study by many investigators [1-7]. A survey of the literature in this area is documented in Ref. [8]. The intricate geometry of the yarns and varying spatial material properties within the fabric makes the response of such composites different from that of unidirectional composites. Most of the analytical studies on such composites have been focussed on predicting its elastic properties [1-7]. Studies relating to prediction of their strength and failure modes are relatively few [9-12]. To understand the behavior and damage mechanisms causing failure of fabric composites, a detailed modeling of the geometry and material properties is necessary. Such modeling is possible by the use of three-dimensional finite elements. Existing modeling tools and FE preprocessors are not adequate for rapidly creating complex 3-dimensional models needed for the purpose. Therefore, mesh generation programs were developed which would easily interface with a general purpose FE analysis software, ABAQUS [13]. FE models can be generated for plain weaves and higher order satin-weaves using a minimal definition of the textile architecture.

Nonlinear material behavior of composites is due to damage accumulation, which causes changes in the stiffnesses of the material. Material nonlinearity combined with high local stress fields can result in a variety of damage mechanisms such as matrix cracking, fiber breakage, and delamination which influence the overall properties of the composite. It is well known that macroscopic failure is preceded by an accumulation of different types of microscopic damage and stiffness losses due to the accumulation of such damage, which cause significant load redistribution. Final failure usually occurs due to the development of one or more areas of highly localized stiffness losses, which behave as macroscopic damages or cracks. Hence, a proper modeling of the damage growth, stiffness loss and load redistribution is essential for a reliable prediction of the weave response.

In the present approach, damages in the composite constituents are modeled on a continuum basis and related to its material constitutive behavior. The 3D constitutive laws describing matrix and yarn behavior are developed using a damage mechanics based approach with the dissipated energy density as the damage parameter. The strain energy dissipation (SED) concept is employed to describe the damage state and current stiffnesses of the weave constituents. The yarns are treated to be transversely isotropic while the pure matrix pockets are assumed to be isotropic.

The developed methodology for geometric and damage modeling in fabric composites is demonstrated through an investigation of progressive failure of plain woven composites subjected to external loads. Two loading conditions are considered viz. in-plane tension and in-plane shear. For a realistic modeling of the weave response, both geometric and material non-linearities are considered. The inititiation and growth of damage within the fabric is investigated and the important stresses causing failure identified.

FABRIC GEOMETRY

For a realistic prediction of the fabric response, a proper modeling of the fabric architecture is essential. Within a woven fabric, the interlaced nature of the yarns causes an asymmetry in distribution of the warp and fill. On one side of the woven fabric, there is a preponderance of warp while the same is true for the fill on the other side. This asymmetry in material distribution causes a coupling of the in-plane and out-of-plane actions. The undulations of the yarns create pockets of space within the fabric, which are filled by the binding matrix. In the current analysis, the yarns are assumed to follow a sinusoidal path, over yarns running orthogonally to them. The yarn path and cross-sectional geometry of the yarns are similar to that described in Ref. [3]. The cross-section profile of the yarns and the undulation path are described in terms of yarn width, yarn count and fiber volume fraction. They provide an adequate representation of the varying cross-sectional profile and undulation of the yarns.

The periodic nature of the yarn undulations makes it possible to identify repetitive portion of the woven fabric. The mechanical response of the fabric can then be described by analyzing such repetitive portions, termed as *unit cell*, of the textile. The *unit cell* with appropriate boundary conditions can thus be used to examine the behavior of the entire textile subjected to various loading conditions. Unit cells of the textile forms considered in the present study are shown in Figure 1.

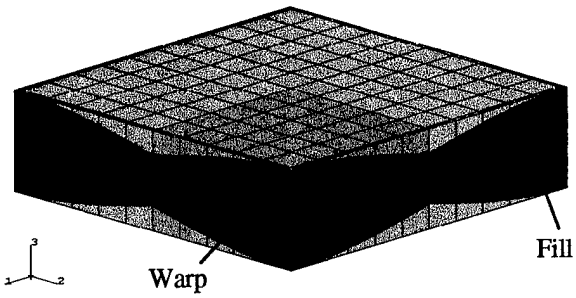

(a)

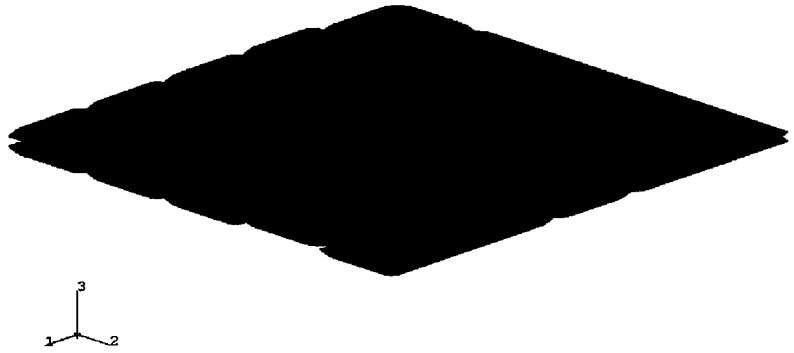

(b)

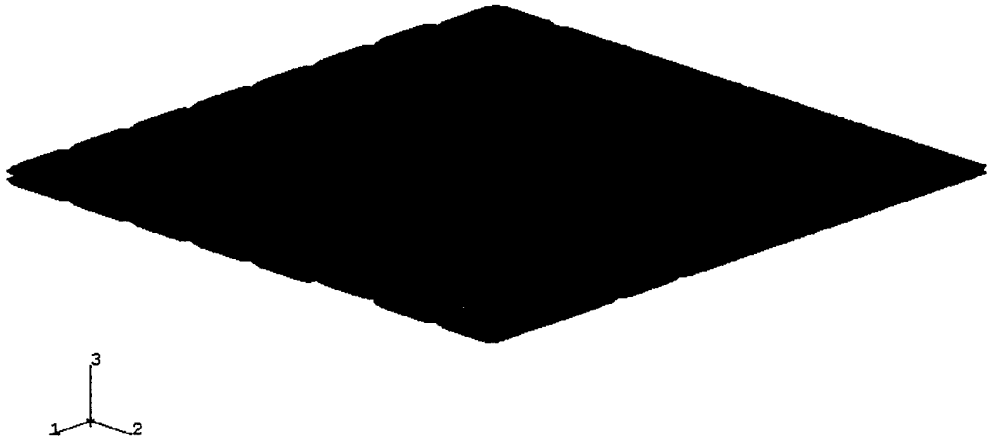

(c)

Figure 1. (a) Plain Weave (one quarter highlighted) (b) 5 Harness Satin (c) 8 Harness Satin

Finite Element Discretization

The weave is analyzed using ABAQUS [13] employing 20 noded, 15 noded and 10 noded three-dimensional elements. An in-house parametric finite element mesh generator described earlier permits an automatic meshing of the weave unit cell and ABAQUS input file generation.

To simulate different loading conditions, appropriate boundary conditions are used (see Appendix D). For the case of plain weaves, symmetry within the periodic cell (Figure 2) can be used to identify the repeating unit cell (Figure 3). Further, the point symmetrical material distribution about the *z*-axis within the unit cell (Figure 3) makes it possible to analyze only one quarter (Figure 4) with appropriate boundary conditions. This results in a reduction of problem size and computational time.

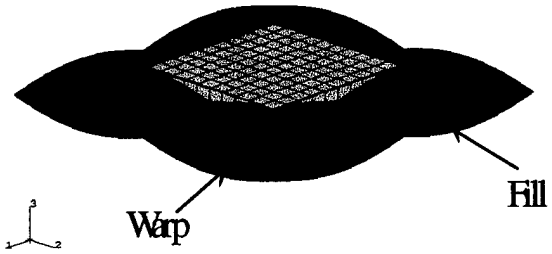

Figure 2. Plain Weave Periodic Cell (some matrix portions removed for clarity)

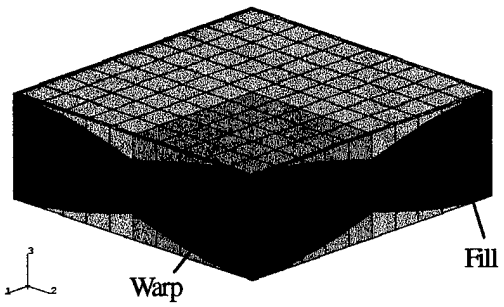

Figure 3. Plain Weave Unit Cell (one quarter highlighted)

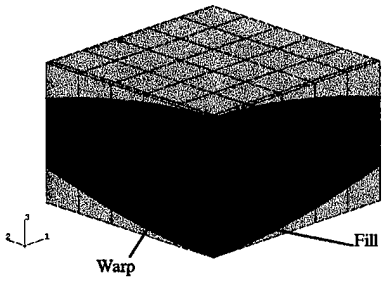

Figure 4. Quarter of Plain Weave Unit Cell

Details of the boundary conditions applicable to the quarter cell plain weave model (Figure 5) are described in Appendix A and are summarized below:

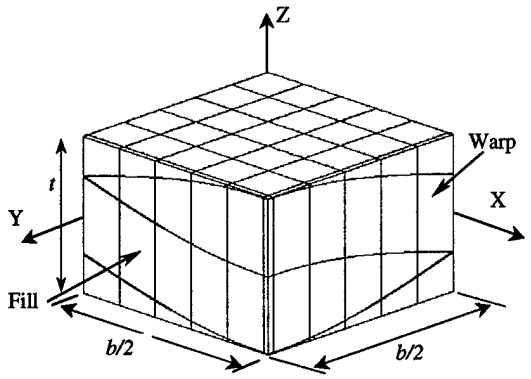

Figure 5. Quarter Cell of Plain Weave

For the case of in-plane extensional loading in the x direction:

$$
\begin{aligned}
&\text{On the plane } x = 0: && u(0,y,z) = -u(0,y,-z)\\
& && v(0,y,z) = v(0,y,-z)\\
& && w(0,y,z) = -w(0,y,-z)\\
&\text{Along the } y-\text{axis } (0,y,0): && u(0,y,0) = 0.0\\
&\text{On the plane } y = 0: && u(x,0,z) = u(x,0,-z)\\
& && v(x,0,z) = -v(x,0,-z)\\
& && w(x,0,z) = -w(x,0,-z)\\
&\text{Along the } x-\text{axis } (x,0,0): && v(x,0,0) = 0.0\\
&\text{Along the } z-\text{axis } (0,0,z): && u(0,0,z) = 0\\
& && v(0,0,z) = 0\\
& && w(0,0,z) = -w(0,0,-z)\\
&\text{On the plane } x = b/2: && u(\frac{b}{2},y,z) = \frac{u_0}{2}\\
&\text{On the plane } y = b/2: && v(x,\frac{b}{2},z) = \text{uniform}
\end{aligned}
\qquad (1)
$$

The boundary conditions for in-plane shear loading are:

$$
\begin{aligned}
&\text{On the plane } x = 0 && u(0,y,z) = u(0,y,-z)\\
& && v(0,y,z) = -v(0,y,-z)\\
& && w(0,y,z) = w(0,y,-z)\\
&\text{On the plane } y = 0 && u(x,0,z) = -u(x,0,-z)\\
& && v(x,0,z) = v(x,0,-z)\\
& && w(x,0,z) = w(x,0,-z)\\
&\text{On the plane } y = \frac{b}{2} && u(x,\frac{b}{2},z) = \frac{p}{2}\\
& && w(x,\frac{b}{2},z) = 0\\
&\text{On the plane } x = \frac{b}{2} && v(\frac{b}{2},y,z) = \frac{p}{2}\\
& && w(\frac{b}{2},y,z) = 0
\end{aligned}
\qquad (2)
$$

ELASTIC ANALYSIS

The boundary conditions shown in Eqns. 1 - 2, along with those described earlier (Appendix D), were used to compute the elastic properties of plain, 5-harness satin and 8-harness weaves to validate the FE model. For the sake of comparison with published analytical and experimental results [3], AS4 Graphite/Epoxy 6501 woven fabrics with a yarn fiber volume fraction of 0.75 were chosen. The width of the yarns was 1.411 mm and its thickness was 0.01 mm. The filament count in both the warp and fill tows was assumed to be 3000 [3]. The material properties of AS4-Graphite fiber and epoxy matrix shown in Table 1 were used to compute the effective elastic properties of the individual yarns using NDPROP [14] and are listed in Table 2. These effective properties of the yarns were used to compute the textile elastic stiffnesses. Table 3 shows a comparison of the current results with other analytical and experimental results for plain, 5-harness and 8-harness satin weaves. For an AS4 graphite/epoxy cross-ply laminate having an overall fiber volume fraction equal to that of the aforementioned weaves (V_f = 0.64), the elastic modulus computed using the CLT theory is 67.60 GPa [3]. It can be seen that the undulation of the yarns causes a reduction in the in-plane extensional stiffness of the weaves and this reduction is maximum in plain weaves where the effect of yarn cross-over is maximum. The effect of mesh discretization on the predicted properties was studied in the case of plain weaves as shown in Table 4.

Table 1. Material Properties of Fiber and Matrix [3]

Material	E_{11} GPa (psi)	E_{22} GPa (psi)	ν_{12}	ν_{23}	G_{12} GPa (psi)
AS4 Graphite	234.43 (3.4×10^7)	22.40 (3.25×10^6)	0.3	0.35	22.064 (3.2×10^6)
Epoxy 3501-6	3.45 (5.0×10^5)	3.45 (5.0×10^5)	0.35	0.35	1.28 (1.85×10^5)

Table 2. Material Properties of the Yarns

Material	E_{11} GPa	E_{22} GPa	ν_{12}	ν_{23}	G_{12} GPa	G_{23} GPa
AS4/Epoxy 6501 ($V_f = 0.64$)	144.8	11.73	0.230	0.30	5.52	3.3

Table 3. Comparison of Present Results with Analytical and Experimental Studies

Textile		E_x GPa (Msi)	E_z GPa (Msi)	ν_{xy}	ν_{zx}	G_{xy} GPa (Msi)	G_{xz} GPa (Msi)
AS4/Epoxy Plain weave ($V_f^o = 0.64$)	Present	62.33 (9.04)	11.84 (1.72)	0.060	0.420	4.7125 (0.68)	3.85 (0.56)
	Experimental [3]	61.92 (8.98)	-	0.110	-	-	-
	FEM [3]	63.78 (9.25)	11.38 (1.65)	0.031	0.329	4.82 (0.69)	4.97 (0.72)
AS4/Epoxy 5-harness satin ($V_f^o = 0.64$)	Present	66.09 (9.58)	11.75 (1.70)	0.050	0.410	4.17 (0.60)	3.85 (0.56)
	Experimental [3]	69.43 (10.06)	-	0.060	-	5.24 (0.76)	-
	FEM [3]	65.99 (9.57)	11.38 (1.65)	0.030	0.320	4.96 (0.72)	5.03 (0.73)
AS4 / Epoxy 8-harness satin ($V_f^o = 0.64$)	Present	66.99 (9.71)	11.57 (1.67)	0.045	0.37	4.462 (0.65)	3.99 (0.57)
	Experimental [3]	72.19 (10.47)	-	0.06	-	6.76 (0.98)	-
	FEM [3]	66.74 (9.68)	11.45 (1.66)	0.03	0.32	4.96 (0.72)	5.03 (0.73)

Table 4. Mesh Refinement Studies (AS4/Epoxy 3501-6 Plain Weave)

	Number of elements	E_x MPa	CPU (seconds)
Periodic cell	400	62.338	28.930
	1296	62.117	273.07
	2704	61.910	2985.5
Quarter cell	36	62.08	2.53

To validate the FE modeling technique further, data on plain weave composites available in literature is considered. Three balanced plain weaves, viz. E-Glass/Epoxy [10], AS4-Carbon/Epoxy [9], and Carbon/Epoxy plain woven fabrics [6], are studied. The boundary conditions described in Eqn. 1 and Eqn. 2 are used to determine the elastic moduli of plain weaves. Table 5 lists the material properties of the constituents of the weaves. The geometrical properties of the woven fabrics used in the computations are shown in Table 6. A comparison of the elastic constants of plain weaves obtained from the present FE model with analytical and experimental results is shown in Table 7. As can be observed, there is a good correlation between the present results and those available in literature. The slight discrepancies in values arise as a result of differences in modeling techniques between the present approach and those adopted in literature.

Table 5. Elastic Properties of Yarns and Matrix Used in the Analysis

Material	Material Property					
	E_{11}	E_{22}	ν_{12}	ν_{23}	G_{12}	G_{23}
	GPa (Msi)	GPa (Msi)			GPa (Msi)	GPa (Msi)
E-Glass/Epoxy [10] (V_f^y=0.65)	48.47 (7.03)	18.06 (2.62)	0.25	0.34	5.58 (0.81)	3.31 (0.48)
AS4-Carbon/Epoxy [9] (V_f^y= 0.70)	155.83 (22.60)	10.13 (1.47)	0.24	0.5	5.72 (0.83)	3.38 (0.49)
Carbon/Epoxy [6] (V_f^y= 0.6)	135.27 (19.61)	9.65 (1.40)	0.28	0.43	5.37 (0.78)	3.38 (0.49)
Epoxy 3502 [9]	3.79 (0.55)	3.79 (0.55)	0.35	0.35	1.38 (0.20)	1.38 (0.20)

Table 6. Geometrical Properties of Yarns

Material	Yarn width mm (in.)	Yarn thickness mm (in.)	Yarn spacing mm (in.)	V_f^y	V_f^o
E-Glass/epoxy [10]	1.747 (0.068)	0.268 (0.010)	1.747 (0.068)	0.65	0.35
AS4-Carbon/epoxy [9]	1.760 (0.069)	0.129 (0.005)	1.760 (0.069)	0.70	0.60
Carbon/epoxy [6]	2.499 (0.0984)	0.109 (0.0043)	2.499 (0.0984)	0.63	0.50

Table 7. Comparison of Present FEA Results With Other Analytical/Experimental Results for Plain Woven Fabrics

Material	Property	Present	Experimental [6,9,10]	Analytical [9,10]
E-Glass/epoxy plain weave [10] $V_f^o = 0.35$	E_x GPa (Msi)	18.88 (2.74)	19.137 (2.775)	19.375 (2.81)
	ν_{xy}	0.14	-	-
	G_{xy} GPa (Msi)	5.972 (0.866)	-	6.142 (0.890)
AS4-Carbon/epoxy plain weave [9] $V_f^o = 0.60$	E_x GPa (Msi)	60.40 (8.760)	60.0 (8.702)	61.250 (8.883)
	ν_{xy}	0.043	-	-
	G_{xy} GPa (Msi)	4.883 (0.708)	4.875 (0.707)	4.861 (0.705)
Carbon/epoxy plain weave [6] $V_f^o = 0.50$	E_x GPa (Msi)	26.1 (3.785)	25.0 (3.62)	-
	ν_{xy}	0.06	-	
	G_{xy} GPa (Msi)	3.56 (0.516)	-	

The reduction in the in-plane stiffness of woven fabrics in comparison with that of unidirectional lamina is influenced to a large extent by the waviness of the yarns. This degree of undulation of the yarns depends on the thickness (h) and width (a) of the yarns. Lower h/a ratio indicates a lower degree of undulation and vice versa. The yarn fiber volume fraction is kept

constant (V_f^y = 0.70). It can be seen that the modulus E_x reduces with increase in h/a values. As h/a values increases, so does undulation. This is accompanied by a lowering of the overall volume fraction (V_f^o). However, the Poisson's ratio decreases with increase in overall volume fraction. Table 8 lists the variation of elastic properties with the degree of undulation (h/a) and the overall fiber volume fraction of the weave. It can be observed that as the undulation decreases, the yarns get compacted leading to an increase in the overall fiber volume fraction. With increase in undulation length, the magnitude of the local fiber angle decreases. This also reduces the coupling between extension and bending effects. The shear modulus increases with increase in the degree of undulation (h/a) of the yarns.

Table 8. Effect of h/a and u/a on Material Properties of AS4-Carbon/Epoxy ($V_f^y = 0.70$) Plain Weave [9]

V_f^o	h mm (in)	a mm (in)	h/a	E_x GPa (Msi)	ν_{xy}	G_{xy} GPa (Msi)
0.45	0.172 (0.006)	1.76 (0.069)	0.098	46.13 (6.69)	0.053	5.134 (0.745)
0.50	0.154 (0.006)	1.76 (0.069)	0.088	51.09 (7.41)	0.049	5.009 (0.726)
0.55	0.143 (0.005)	1.76 (0.069)	0.082	54.95 (7.97)	0.046	4.943 (0.717)
0.60	0.129 (0.005)	1.76 (0.069)	0.074	60.40 (8.76)	0.044	4.883 (0.708)
0.65	0.119 (0.004)	1.76 (0.069)	0.068	65.02 (9.43)	0.041	4.854 (0.703)
0.70	0.111 (0.004)	1.76 (0.069)	0.064	72.40 (10.5)	0.036	4.863 (0.705)

FABRIC STRESS DISTRIBUTIONS

A study of the internal stress distributions generated within the fabric when subjected to external loads is carried out. This would be useful in identifying the dominant ones and also regions of stress concentrations. This information would aid in predicting possible modes of damage likely to occur within the yarns and surrounding pure matrix pockets. Such a study would also help in assessing the applicability of damage models for describing the nonlinear behavior of yarn and pure matrix pockets.

For the sake of conciseness, only the important stresses generated within plain weave fabrics as a result of tensile loading are discussed here. The carbon/epoxy plain weave (V_f^o = 0.5) considered earlier is subjected to tension along the warp direction. Plots of the stresses generated in the warp and fill corresponding to an overall applied stress σ_{11}^o = 183.7 MPa (26.64 ksi) are shown in Figures 6 - 11. All the yarn stresses are measured with respect to the local material axes. It can be seen that at regions close to the point where there is a change in curvature of the warp, high values of in-plane shear stress τ_{12} and σ_{11} are prevalent. Such stress concentrations can trigger localized damage in the warp even when the overall applied stress (σ_{11}^o) is much below the final strength of the weave. The out-of-plane normal stresses σ_{33} developed in the warp, though smaller in comparison with the in-plane stresses σ_{11} (peak σ_{33} = 4.682 MPa (0.679 ksi) against a peak σ_{11}= 454.64 MPa (65.938 ksi)) can cause some damage in the yarns. The variation of the in-plane normal stress (σ_{11}) across the thickness of the warp indicates localized bending occurring as a result of extension. Also, small regions can be seen where the local in-plane stresses (σ_{11} and τ_{12}) are very high. The transverse normal stress (σ_{22}) in the fill (orthogonal to the direction of loading) is higher than that in the warp and hence transverse tensile failure in fill would occur much before final failure of the weave.

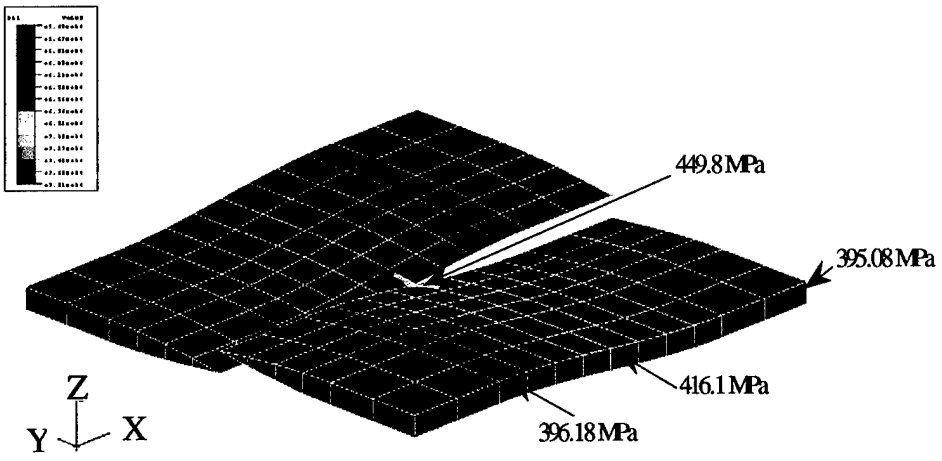

Figure 6. Tensile Stress (σ_{11}) Developed in Warp of Carbon/Epoxy (V_f = 0.5) Subjected to Tension Along Warp Corresponding to Overall Applied Tensile Stress of 183.7 MPa.
(All stresses in MPa and are measured with reference to the local material axes)

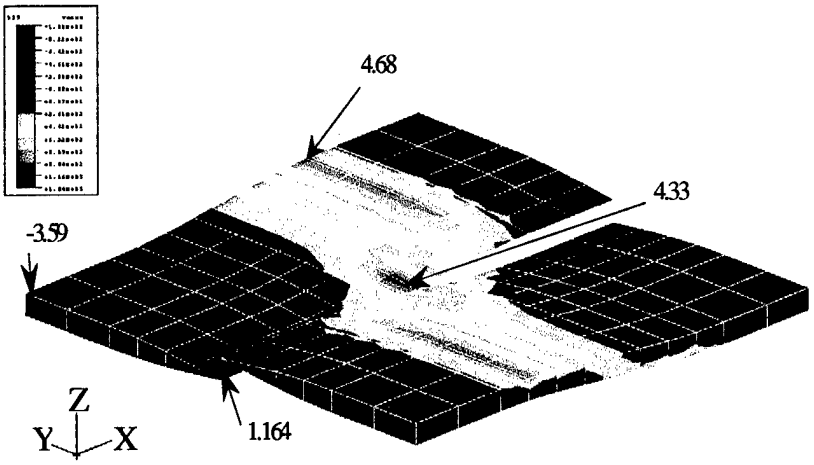

Figure 7. Out-of-Plane Stress (σ_{33}) Developed in Warp of Carbon/Epoxy (V_f = 0.5) Subjected to Tension Along Warp Corresponding to Applied Overall Tensile Stress of 183.7MPa.
(All stresses in MPa and are measured with reference to the local material axes)

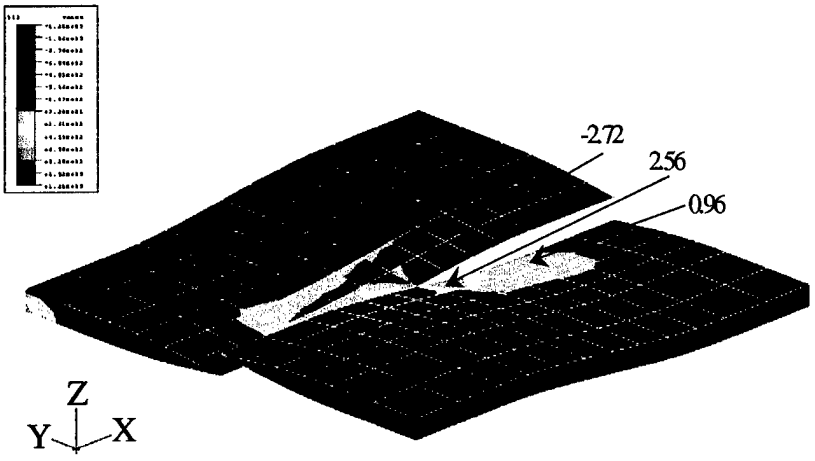

Figure 8. In-Plane Shear Stress (σ_{12}) Developed in warp of Carbon/Epoxy (V_f = 0.5) Subjected to Overall Tensile Stress of 183.65 MPa (26.64 ksi).
(All stresses in MPa and are measured with reference to the local material axes)

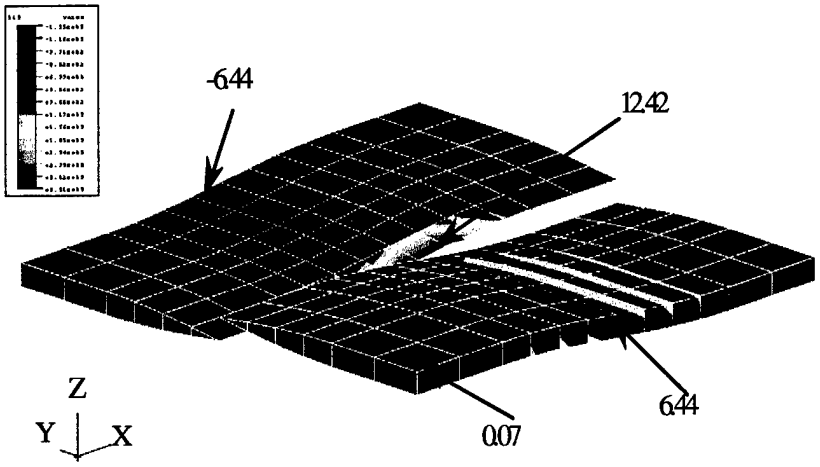

Figure 9. In-Plane Shear Stress (σ_{13}) Developed in Warp of Carbon/Epoxy (V_f = 0.5) Subjected to Overall Tensile Stress of 183.65 MPa (26.64 ksi). (All stresses in MPa and are measured with reference to the local material axes)

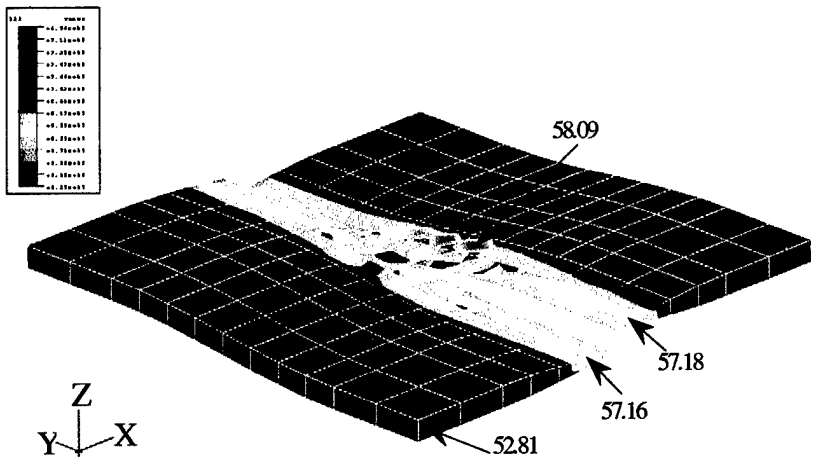

Figure 10. Transverse Normal Stress (σ_{22}) Developed in Fill of Carbon/Epoxy (V_f = 0.5) Subjected to Overall Tensile Stress of 183.65 MPa. (All stresses in MPa and are measured with reference to the local material axes)

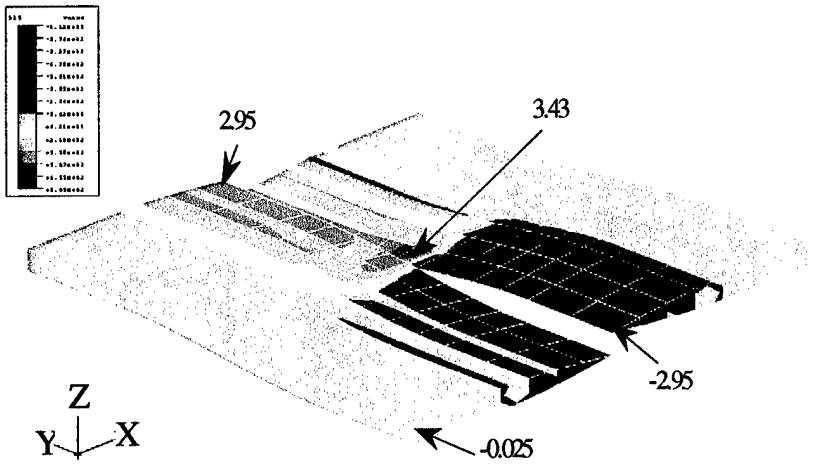

Figure 11. Transverse Shear Stress (τ_{23}) Developed in Fill of Carbon/Epoxy (V_f= 0.5) Subjected to Overall Tensile Stress of 183.65 MPa (26.64 ksi). (All stresses in MPa and are measured with reference to the local material axes)

MATERIAL MODELING

The nonlinear behavior of the weave constituents, viz. yarns and pure matrix, is modeled using a damage mechanics based approach. The dissipated energy density (ϕ) is chosen as the damage parameter. As discussed in Appendix B, the nature of a damage surface for a fixed value of ϕ and its change with ϕ can be modeled at various levels of complexity to simulate the "in-situ" nonlinear material behaviors. In the results reported here, simple quadratic forms of the damage surfaces in terms of chosen strain variables are employed. The changes of these surfaces with ϕ are chosen in a manner such that they yield power law type stress-strain relations under unidirectional straining beyond the initial elastic domain as described in Appendix B. The material characterization curves for AS4-Carbon/Epoxy and E-Glass/Epoxy unidirectional lamina predicted by the current methodology compare well with experimental results contained in References [15] and [16], respectively. The nonlinear behavior of the textile constituents used in the present analyses is shown in Figures 12 –17.

The material constitutive laws for yarns and pure matrix described in Appendix B are incorporated as a user subroutine in ABAQUS [13]. The material properties required for analyses are the elastic moduli, Poisson's ratios and variables that describe the damage surfaces in the strain space for various values of dissipated energy density ϕ in the yarn/matrix.

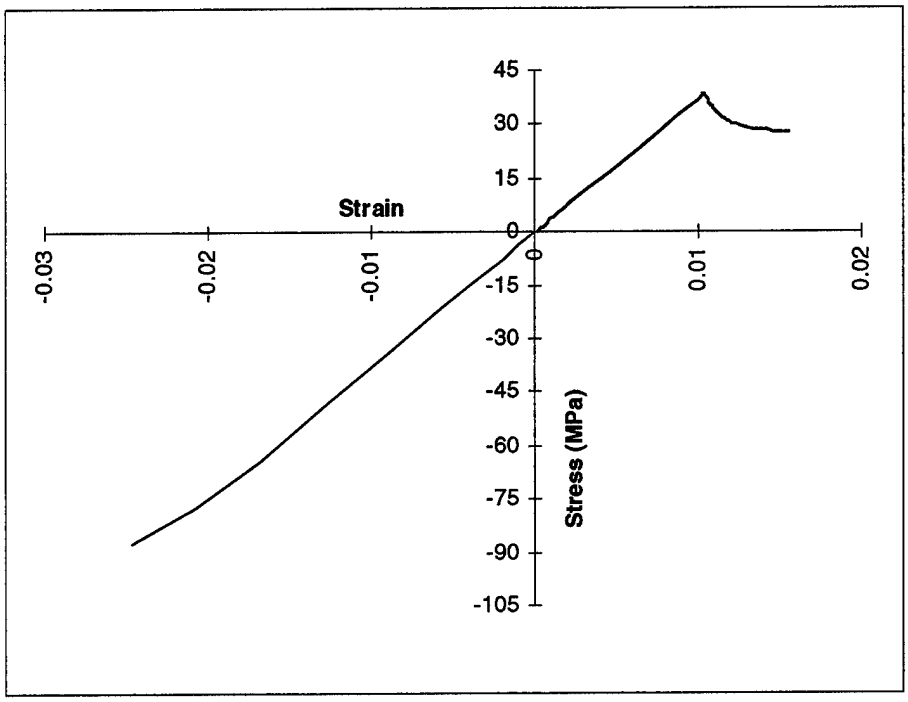

Figure 12. Longitudinal Stress-Strain Curve for Epoxy 3502

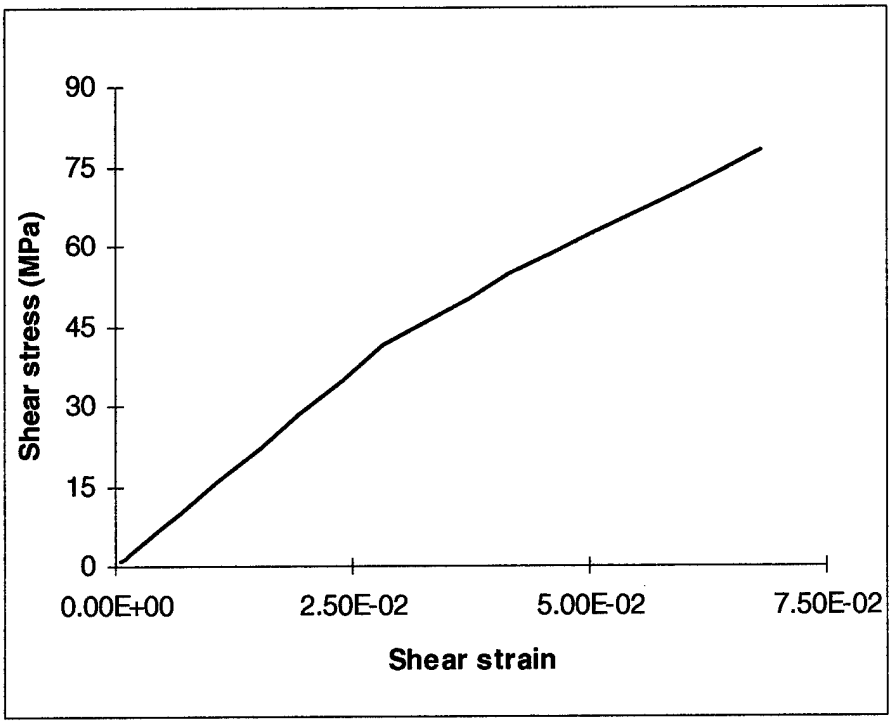

Figure 13. Shear Stress-Strain Curve for Epoxy 3502

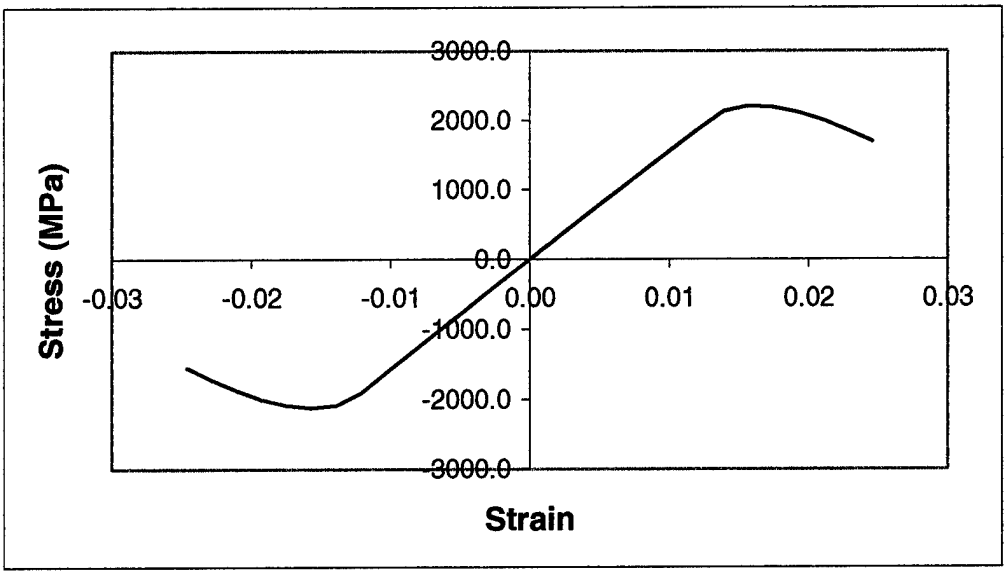

Figure 14. Longitudinal Stress-Strain Curve for AS4/Epoxy ($V_f = 0.7$)

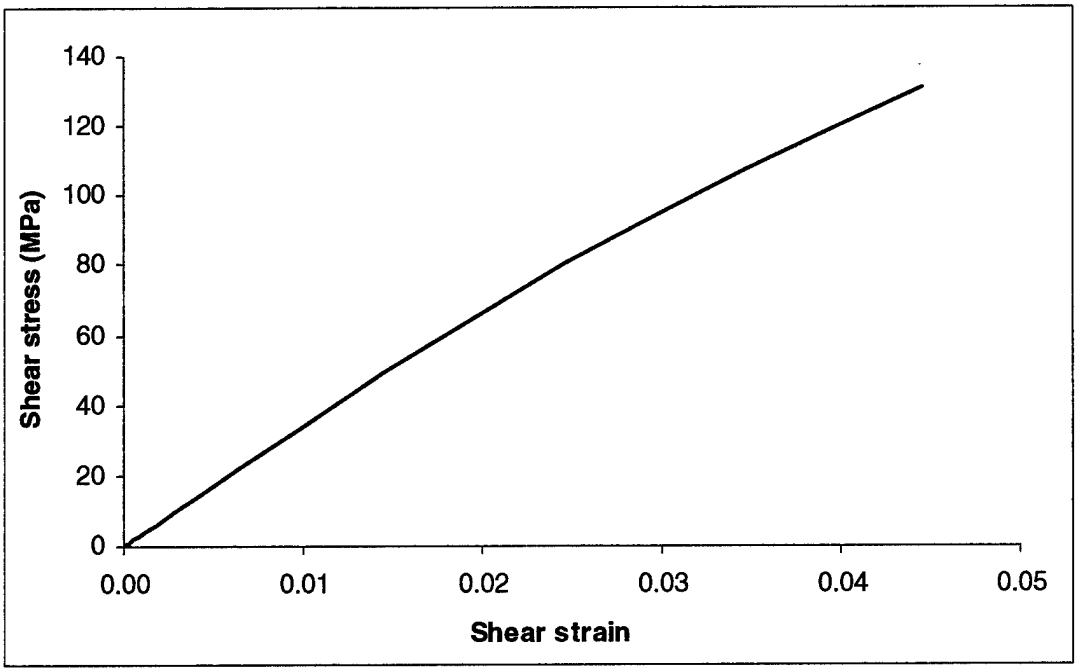

Figure 15. Shear Stress-Strain Curve for AS4/Epoxy ($V_f = 0.7$)

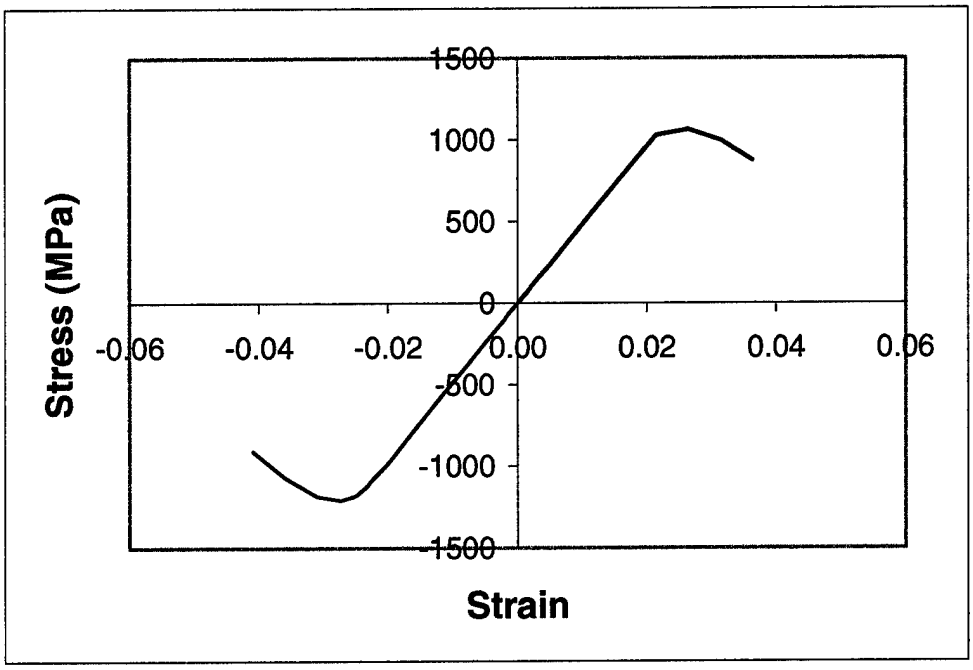

Figure 16. Longitudinal Stress-Strain Curve for E-Glass Epoxy ($V_f = 0.65$)

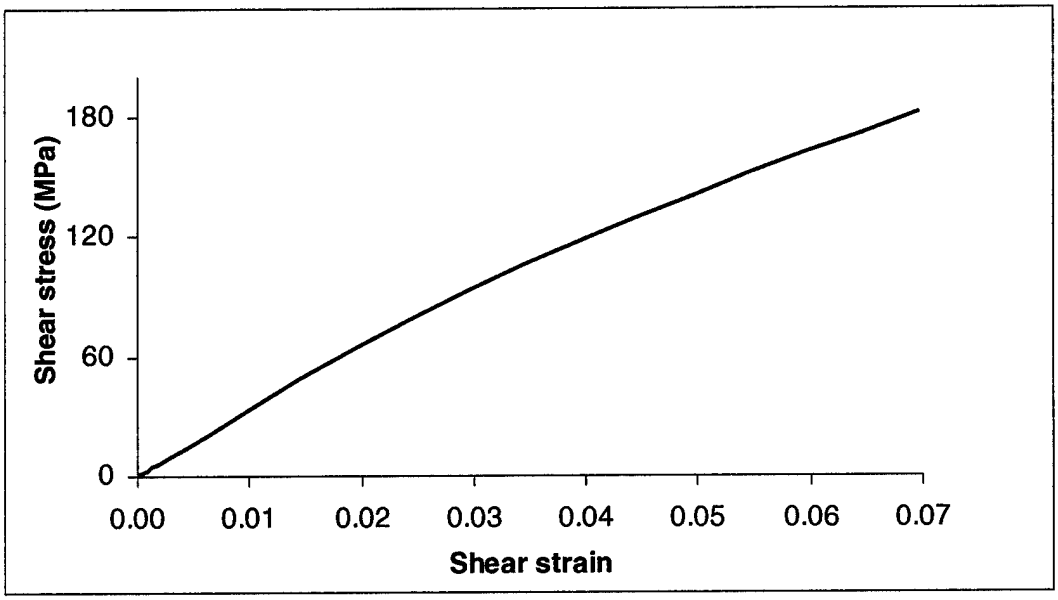

Figure 17. Shear Stress-Strain Curve for E-Glass/Epoxy ($V_f = 0.65$)

NONLINEAR ANALYSIS

A typical unit cell of plain weave discretized by finite elements is shown in Figure 3. Within each finite element of the unit cell, the stiffnesses, stresses and strains can be monitored at the material integration points. This function is performed by the material models described in Appendix B. For this purpose, the constitutive laws for the materials are implemented through a user-defined subroutine (UMAT) and linked with the finite element analysis program, ABAQUS [13]. During each load increment of the nonlinear analysis process, the material definition routines describe the current stiffnesses and damage state at the numerical integration points of the finite elements. The reductions in stiffnesses occurring as a result of localized damage within the yarn/pure matrix pockets are monitored and incorporated into the weave response.

An incremental-iterative approach is adopted for the nonlinear finite element analysis. The modified Newton-Raphson method is used to trace the loading path of the structure. The nonlinear analysis starts from an equilibrium state. Loads are applied by prescribing incremental displacements and the unbalanced forces evaluated. An iterative procedure is used until the out-of-balance load vector or the displacement increments are sufficiently small. Within each element representing yarn/pure matrix, each Gaussian integration point represents a certain volume of material whose material stiffnesses are described by the user material definition subroutine developed. Thus, for a particular increment of load, depending on the current value of the dissipated energy density ϕ, an element may contain some points with no damage and some with damage. Within each load increment of the nonlinear analysis, the material is checked for occurrence of damage. Once damage is detected, the material properties are changed accordingly. At any given stage of loading, the above approach of detecting damage is applied at all Gaussian integration points of the yarn/pure matrix elements. Thus, by modeling damage at discrete integration points, the progressive failure of the woven fabric is analyzed.

The behavior of balanced E-Glass/Epoxy [10] and AS4-Carbon/Epoxy [9] and carbon/epoxy [6] plain woven fabric, described earlier, when subjected to in-plane loads is examined. The current predictions are compared with experimental results if available or with other theoretical results available in literature. Elastic properties of the weave constituents are tabulated in Table 5. The geometrical parameters of the weave used in the present investigation are listed in Table 6.

TENSILE BEHAVIOR

The plain woven fabrics are subjected to tensile loading along warp using boundary conditions described in Eqn. 1. Effects of geometric nonlinearity and material nonlinearity of the yarns and surrounding pure matrix are included in the analysis. Figures 18 and 19 show the stress/strain curves obtained from the present FE analysis.

These results are compared with experimental values [6, 9, 10]. Figure 18 shows a good agreement between the results of the present analysis and experimental values in the pre-'knee' portion of the stress-strain curve. The 'knee' in the stress-strain curve is caused due to transverse tensile failure in the fill.

Carbon/epoxy unidirectional lamina is stiffer than E-Glass/Epoxy lamina. As a result, intermediate damage mechanisms (e.g., 'knee') prior to fracture of fiber are not seen in the stress/strain response of AS4-Carbon/Epoxy plain weave (Figure 19) as clearly as that in E-Glass/epoxy plain weave (Figure 18). Hence, the stress/strain plot is almost linear until final failure. On the other hand, in the case of E-Glass/Epoxy plain weave, the 'knee' is more pronounced than that in AS4-Carbon/Epoxy plain weave. The damage mechanisms seen in the plain weaves subjected to tension along warp direction are: (i) Transverse tensile failure (of matrix) in fill; (ii) Matrix failure in in-plane shear in fill near the yarn extremities where there is a stress concentration; and (iii) Fiber failure in tension in warp.

Figure 20 shows the behavior of carbon/epoxy plain weave lamina [6] subjected to tension along warp and tension along an off-axis ($\theta = 15°$) direction. The progression of damage within the fabric when the fabric is subjected to tension along warp is shown by contour plots of the damage parameter ϕ in Figures 21-25. For the case of off-axis loading, considerable shear softening occurs in the transverse fill before final failure of the weave. Damage in the fill due to transverse tension occurs much earlier (177 MPa) than the damage in the warp caused by fiber failure. The damage mechanisms seen in the plain weave subjected to off-axis tension are: (i) Transverse tensile failure (of matrix) in fill; (ii) Matrix failure in shear in fill; and (iii) Fiber failure in tension in warp.

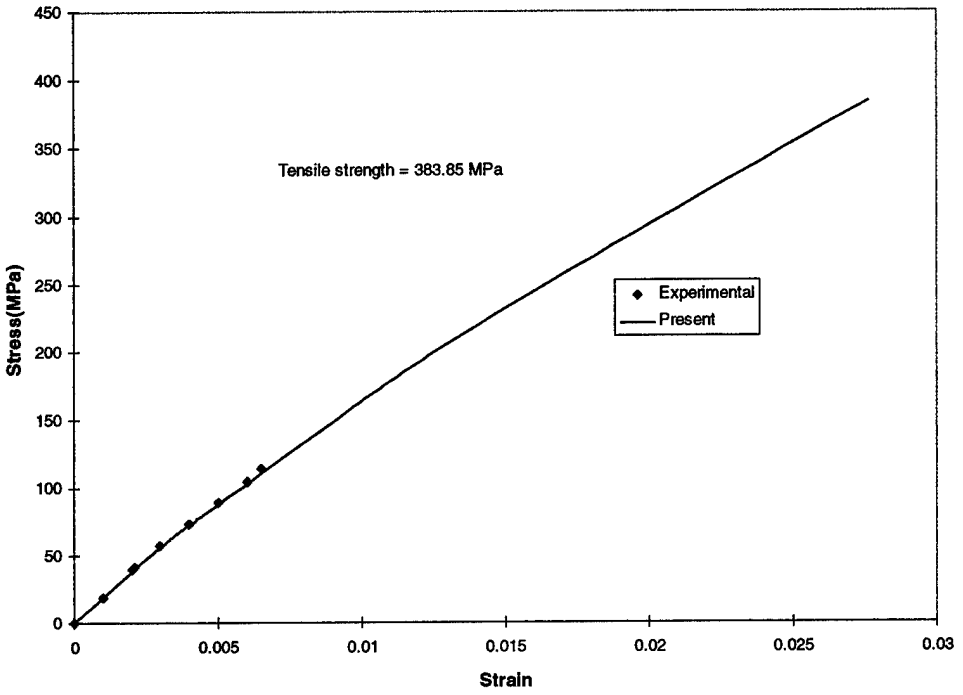

Figure 18. Response of E-Glass/Epoxy Plain Weave Subjected to Tension

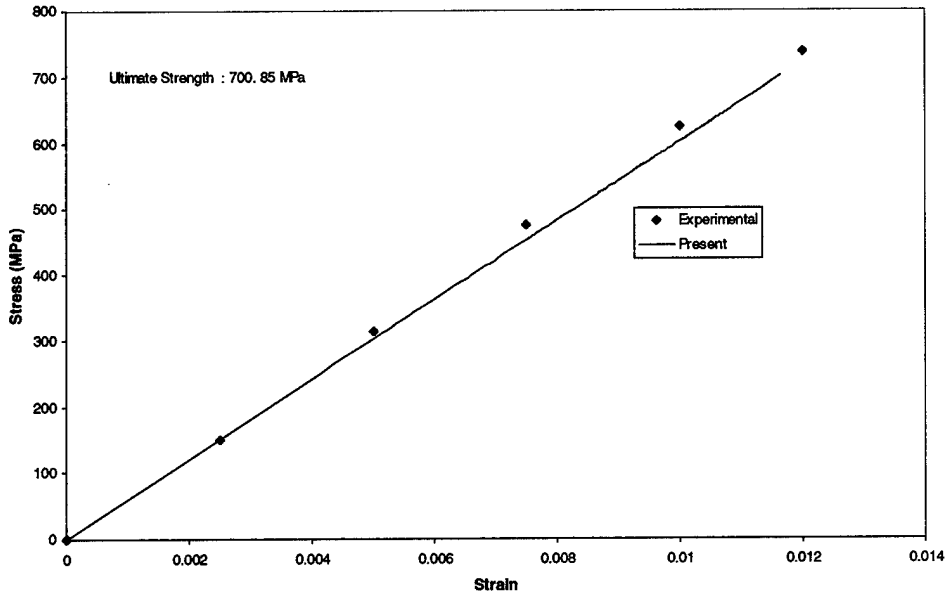

Figure 19. Response of AS4/Carbon/Epoxy Plain Weave Subjected to Tension

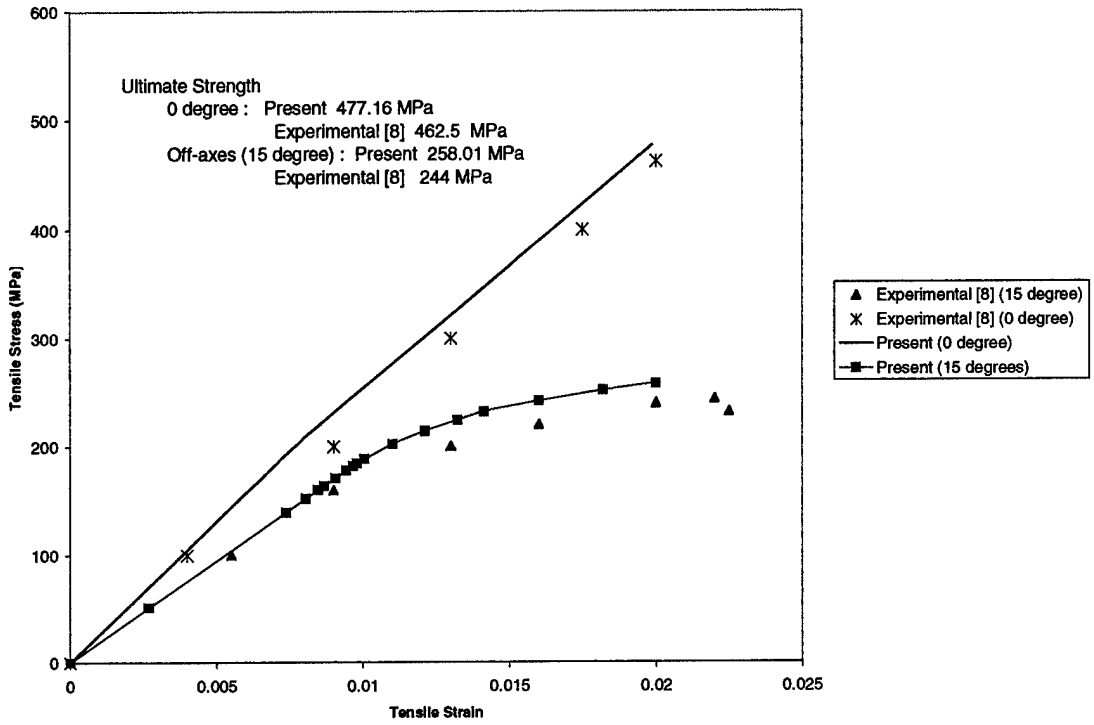

Figure 20: Response of Carbon/Epoxy [6] Plain Weave Subjected to Tension

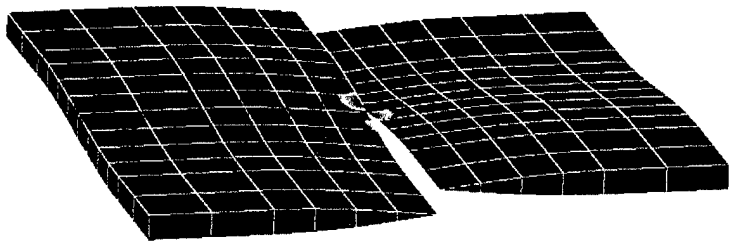

Figure 21. Variation of ϕ in Fill of Carbon/Epoxy Plain Weave Subjected to Tension Along Warp (σ_o = 168.10 Mpa)

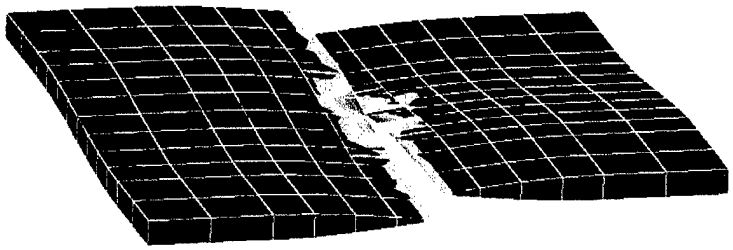

Figure 22. Variation of ϕ in Fill of Carbon/Epoxy Plain Weave Subjected to Tension Along Warp (σ_o = 188.9 MPa)

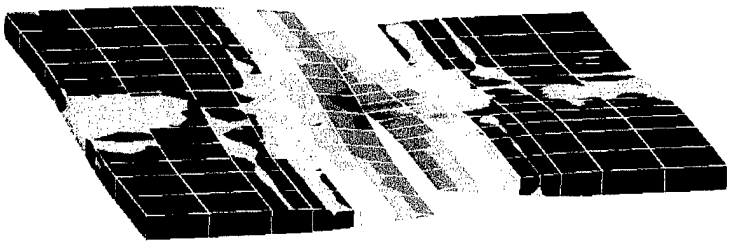

Figure 23. Variation of ϕ in Fill of Carbon/Epoxy Plain Weave Subjected to Tension Along Warp (σ_o = 210.05 MPa)

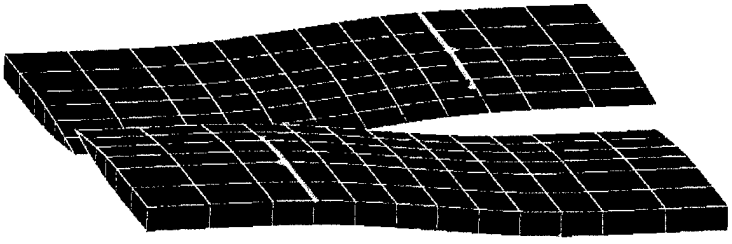

Figure 24. Variation of ϕ in Warp of Carbon/Epoxy Plain Weave Subjected to Tension Along Warp (σ_o = 421.63 MPa)

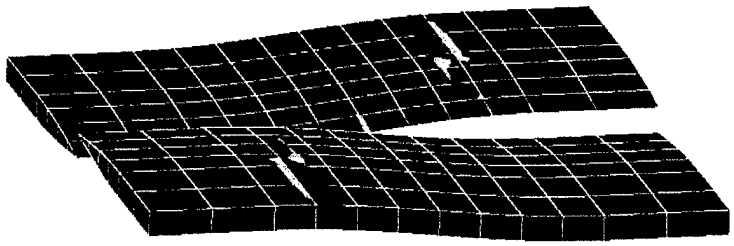

Figure 25. Variation of ϕ in Warp of Carbon/Epoxy Plain Weave Subjected to Tension Along Warp (σ_o = 433.12 MPa)

IN-PLANE SHEAR

The behavior of E-Glass/Epoxy and AS4-Carbon/Epoxy plain weaves under in-plane shear is examined using boundary conditions shown in Eqn. 2. Figures 20 and 21 show the stress-strain curves obtained from the present analysis. For the case of AS4-Carbon/Epoxy plain weave, the present results are compared with an experimental result available in literature [9]. The ultimate strength prediction agrees well with the experimental result though the failure strains differ. This could be due to differences in material properties used in the present material model and those tested. The sequence of failure for plain weaves subjected to in-plane shear is: (i) Matrix failure in shear in fill; (ii) Matrix failure in out-of-plane shear in warp; and (iii) Matrix failure in transverse tension in fill.

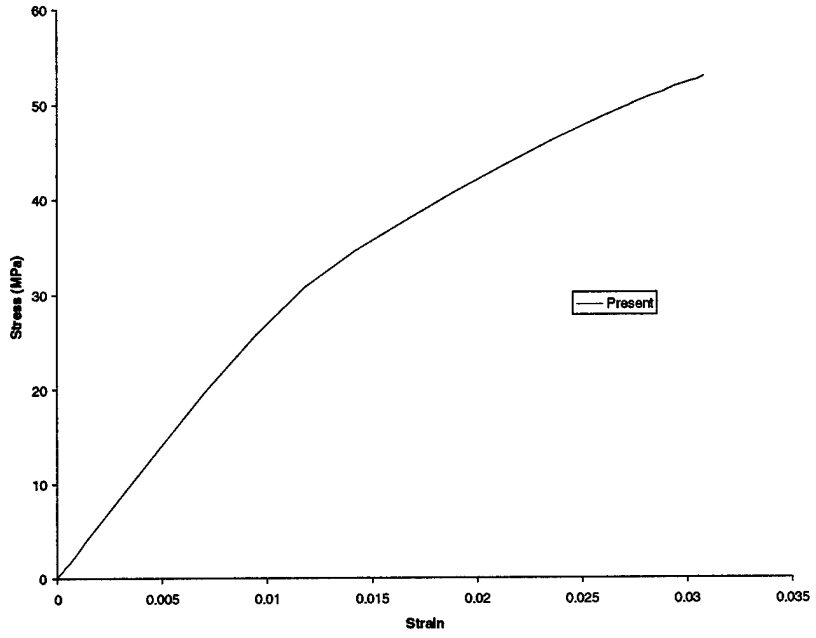

Figure 26. Response of E-Glass/Epoxy Plain Weave Subjected to In-Plane Shear

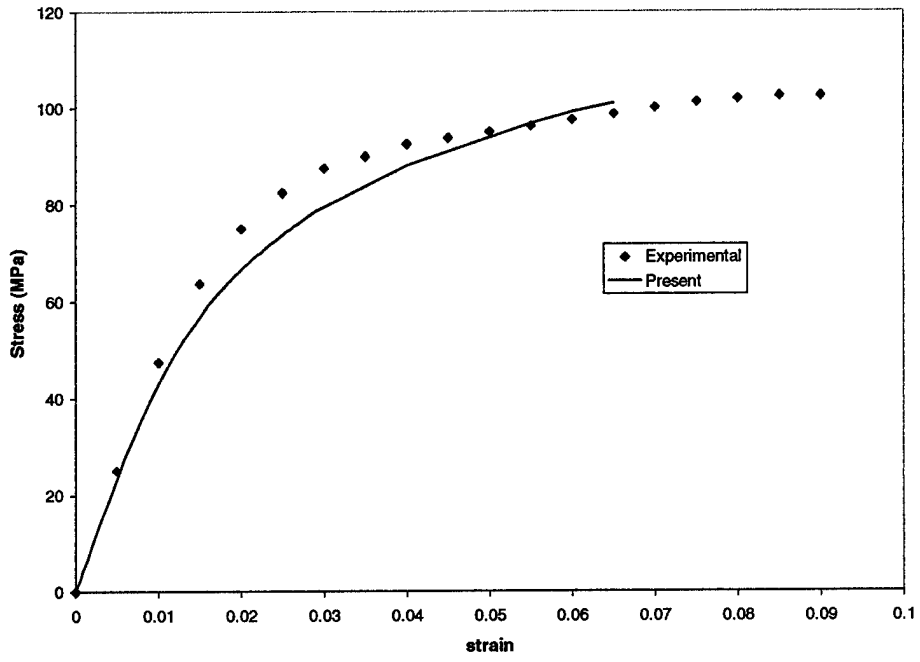

Figure 27. Response of AS4-Carbon/Epoxy Plain Weave Subjected to In-Plane Shear

CONCLUSIONS

An investigation into the micromechanics of fabric composites requires a proper description of the fabric architecture and varying material properties. This has been accomplished by the use of 3D finite elements which permits a detailed modeling of the varying cross-sectional profile and undulations of the yarns. The mesh generation routines which have been developed in the current study can be used to generate FE models for a variety of woven fabrics. The output from the mesh generation programs serve as input files for a general-purpose finite element analysis program, ABAQUS.

The periodic nature of the weave pattern combined with point symmetry of material distribution can be used advantageously in the analysis. This results in a reduction of the problem size and enhances computational efficiency.

A study of the stress distributions generated within the fabrics indicates the presence of concentrations of high values of stress in regions with sharp changes in yarn curvature. This would lead to localized damage even at stresses much below the ultimate strength of the weave. Hence, material models which monitor the onset of damage and accordingly reflect them appropriately in the properties of the fabric constituents are necessary.

Damage mechanics based constitutive laws based on strain energy dissipation ϕ as the damage parameter is developed. The nature of damage surface for a particular value of ϕ and its change with ϕ is modeled to simulate the "in-situ" nonlinear material behaviors. In the present study, simple quadratic forms of the damage surfaces in terms of chosen strain variables are employed. The changes of these surfaces with ϕ are chosen in a manner such that they yield power law type stress-strain relations under unidirectional straining beyond the initial elastic domain. The material model has been used to study and describe the initiation and growth of damage in plain woven fabrics. The damage modeling methodology presented herein has wide applicability in describing response of materials which do not show any rate dependent or viscous behavior.

A progressive failure analysis of plain woven fabrics subjected to in-plane loading has been undertaken and the results compared with analytical/experimental results in literature. Both material and geometric nonlinearities are considered. Plain weaves, when subjected to tension, exhibit an almost linear behavior prior to failure. The dominant failure mechanism is transverse tensile failure of the fill for a plain weave loaded in the warp direction. Such failure causes a reduction in the stiffness of the plain weave and is reflected as a 'knee' in the stress-strain plot.

Plain woven fabrics exhibit a nonlinear behavior when subjected to in-plane shear. This nonlinear behavior is mainly due to the shear softening of matrix in the yarns. Failure of matrix in warp due to in-plane shear and transverse tensile failure of the fill are prime mechanisms of failure under such loading conditions.

PERSONNEL SUPPORTED

GERALD V. FLANAGAN

M.S., Aeronautical Engineering, Air Force Institute of Technology (1983)
B.S., Massachusetts Institute of Technology (1979)

Mr. Flanagan joined MSC in 1994. His duties include project management and development of structural analysis methods. Prior to joining MSC, Mr. Flanagan spent 10 years at Grumman Aircraft Systems. At Grumman, he was responsible for planning and conducting many of the in-house research activities related to composite structures. He was responsible for many of the analysis codes in use at Grumman, managed material test activities, and participated in several large scale composite structures programs. These included the Lavi composite wing, C-17 control surfaces, Boeing 777 control surfaces, composite helicopter components, the DARPA Dry-Deck Shelter, and Grumman's proposal for the Navy AX aircraft. He has made significant contributions in the areas of solution methods for three-dimensional analysis of laminates, structural stability of composite shells, delamination and damage tolerance of laminates, and the analysis of bonded joints.

From 1981 to 1983, Mr. Flanagan was in the U.S. Air Force, assigned to Wright Patterson AFB Materials Laboratory. There, he worked on laminate strength optimization algorithms. Prior to that assignment, he was a technical intelligence analyst, specializing in high-speed propulsion. While at the Massachusetts Institute of Technology, he worked in the Technical Laboratory for Advanced Composites.

Mr. Flanagan has authored numerous papers and reports related to the analysis of composite structures, and is a member of AIAA and ASC.

SAILENDRA N. CHATTERJEE

Ph.D., Engineering Science, University of Mississippi (1971);
M.S., Structural Engineering, Indian Institute of Technology (1965);
B.S., Civil Engineering, University of Calcutta (1962).

Since joining MSC in 1974, Dr. Chatterjee has been active in research, development and

design with various types of composites with thermoset, thermoplastic, metal and ceramic matrices as well as carbon-carbon materials. Dr. Chatterjee has been involved in studies on thermomechanical behavior, dynamic response, wave propagation, NDE, as well as environmental effects and effects of defects on composite structures.

From 1965 to 1968, Dr. Chatterjee was a Lecturer at the Indian Institute of Technology in Bombay, doing research and teaching in the area of engineering mechanics including structural analysis and design of plates and shells. During the next five years, he studied stress analysis and fracture mechanics as a Researcher and Postdoctoral Research Associate at the University of Mississippi and then as an NRC Resident Research Associate at the Mechanics Research Lab, AMMRC. In the capacity of Senior Research Fellow at the Indian Institute of Science from 1973 to 1974, his research and teaching was in the area of mechanics of solids, stress analysis, and fracture mechanics.

Dr. Chatterjee is a member of ASME, ASCE, ASTM and AIAA, and has written more than fifty papers on stress analysis, fracture mechanics, and composites.

MANOHAR G. KOLLEGAL

Ph. D., Structural Engineering, Washington University, St. Louis (1998);
M. S., Structural Engineering, Indian Institute of Technology, Bombay (1993);
B. S., Civil Engineering, Victoria Jubilee Technical Institute, Bombay (1991).

Dr. Kollegal joined MSC in 1998. His duties include investigating the micromechanics of textile composites and the development of finite element mesh generation codes for woven and braided composites.

Prior to joining MSC, as a Research Assistant at Washington University, he was involved in research and teaching in the areas of structural mechanics, composite materials and experimental techniques. During 1993, while at the R&D division of Tata Consulting Engineers at Bombay, he developed structural design methodologies and software tools for analysis and design of structures.

Dr. Kollegal is a member of ASCE and SAMPE

PUBLICATIONS

"Progressive Failure Analysis of Plain Weaves Using Damage Mechanics Based Constitutive Laws", submitted to International Journal of Damage Mechanics, Technomic Publishing Co., Inc.

INTERACTIONS/TRANSITIONS

There were no meetings, consultations, or transitions to report in this period.

NEW DISCOVERIES, INVENTIONS, OR PATENT DISCLOSURES

None.

HONORS/AWARDS

None.

REFERENCES

1. Chou, T. W. (1992), Microstructural Design of Fiber Composites, Cambridge University Press, Cambridge, UK.
2. Dow, N. F., Ramnath, V and Rosen, B. W. (1987), Analysis of Woven Fabrics for Reinforced Composite Materials, NASA-CR-178275, NASA, Hampton, Virginia.
3. Naik, R. A. (1994), *Analysis of Woven and Braided Fabric Reinforced Composites*, NASA CR 194930, NASA, Hampton, Virginia.
4. Kuhn, J. L and Charalambides, P. G. (1998), *Elastic Response of Porous Matrix Plain Weave Fabric Composites: Part I-Modeling*, Journal of Composite Materials, Vol. 32, No. 16, pp. 1426-1471.
5. Kuhn, J. L and Charalambides, P. G. (1998), *Elastic Response of Porous Matrix Plain Weave Fabric Composites: Part II-Results*, Journal of Composite Materials, Vol. 32, No. 16, pp. 1472-1508.
6. Naik, N. K. (1994), *Woven Fabric Composites*, Technomic Pub. Co., Lancaster, PA.
7. Whitcomb, J. D. (1989), Three-dimensional Stress Analysis of Plain Weave Composites, Paper presented at the *3rd Symposium of Composite Materials: Fatigue and Fracture*, Orlando, Florida, October 1989. ASTM STP n 1110, 1991.
8. Cox, B. N. and Flanagan, G. (1997), *Handbook of Analytical Methods for Textile Composites*, NASA CR 4750, NASA, Hampton, Virginia.
9. Blackketter, D. M., Walrath, D. E., and Hansen, A. C., (1993), *Modeling Damage in a Plain Weave Fabric-Reinforced Composite Material*, Journal of Composites Technology and Research, 15, No. 2, pp. 136-142.
10. Dasgupta A. and Bhandarkar S. M. (1994), *Effective Thermomechanical Behavior of Plain-Weave Fabric Reinforced Composites Using Homogenization Theory*, Journal of Engineering Materials and Technology, Transactions of the ASME, 116, pp. 99-105.
11. Makoto, I. and Chou, T. W. (1998), *An Analytical and Experimental Study of Strength and Failure Behavior of Plain Weave Composites*, Journal of Composite Materials, Vol. 32, No. 1, pp. 2-30.
12. Naik, A. R. (1994), Failure Analysis of Woven and Braided Fabric Reinforced Composites, NASA-CR-194981, NASA, Hampton, Virginia.
13. ABAQUS, ver 5.7, Hibbitt, Karlsson & Sorensen, Inc., Pawtucket, RI.
14. NDP 9.2 General Composites Analysis, Ver. 6.0, Materials Sciences Corporation, PA.

15. Chatterjee, S. N., Wung, E. C. J., Yen, C. F., Ramnath V., Kesler, J. A. and Adams, D. F. (1991), *Composite Specimen Design Analysis, Vol. I: Analytical Studies, Vol. II: Experimental Effort*, MTL TR 91-5.
16. Clements, L. L. and Moore, R. L. (1978), *Composite Properties for E-Glass in a Room-Temperature Curable Epoxy Matrix*, Composites, Vol. 9, No. 2.
17. Hashin, Z., (1983), *Analysis of composite materials -A survey*, Journal of Applied Mechanics, Vol. 105, pp. 481-505.

APPENDIX A – BOUNDARY CONDITIONS

Suite 250, 500 Office Center Drive
Fort Washington, PA 19034
Tel: 215-542-8400 Fax: 215-542-8401

APPENDIX A - BOUNDARY CONDITIONS

The boundary conditions for a periodic cell of balanced woven fabric are first stated. The woven fabric is assumed to be a part of a laminate in which successive woven fabrics are stacked symmetrically about the xy plane.

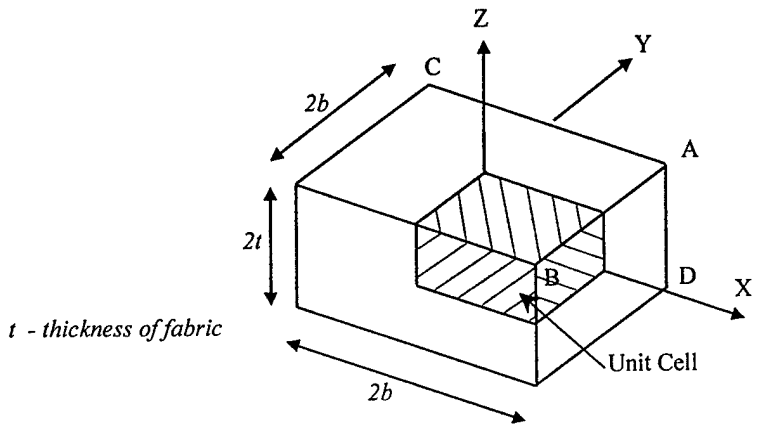

Figure A1. Periodic Cell

The conditions which need to be satisfied on account of the periodic nature of the weave geometry are (Figure A1):

On the planes $x = \pm b$,

$$\begin{aligned} u(b,y,z) - u(-b,y,z) &= u_A - u_C \\ v(b,y,z) - v(-b,y,z) &= v_A - v_C \\ w(b,y,z) - w(-b,y,z) &= w_A - w_C \end{aligned} \qquad \text{(A1)}$$

On the planes $y = \pm b$,

$$\begin{aligned} u(x,b,z) - u(x,-b,z) &= u_A - u_B \\ v(x,b,z) - v(x,-b,z) &= v_A - v_B \\ w(x,b,z) - w(x,-b,z) &= w_A - w_B \end{aligned} \qquad \text{(A2)}$$

On the planes $z = \pm t$,

$$\begin{aligned} u(x,y,t) - u(x,y,-t) &= u_A - u_D \\ v(x,y,t) - v(x,y,-t) &= v_A - v_D \\ w(x,y,t) - w(x,y,-t) &= w_A - w_D \end{aligned} \qquad \text{(A3)}$$

A1.1 BOUNDARY CONDITIONS FOR IN-PLANE EXTENSION

A1.1.1 Boundary Conditions for Unit Cell

An extension along the x-axis is prescribed such that

$$\begin{aligned} u_A &= -u_C = u_o \\ v_A &= -v_B = v_o \\ w_A &= -w_D = w_o \end{aligned}$$

The periodic conditions for extension from Eqns A1-A3 are:

On the planes $x = \pm b$,

$$\begin{aligned} u(b,y,z) - u(-b,y,z) &= 2u_o \\ v(b,y,z) - v(-b,y,z) &= 0 \\ w(b,y,z) - w(-b,y,z) &= 0 \end{aligned} \qquad \text{(A4)}$$

On the planes $y = \pm b$,

$$\begin{aligned} u(x,b,z) - u(x,-b,z) &= 0 \\ v(x,b,z) - v(x,-b,z) &= 2v_o \\ w(x,b,z) - w(x,-b,z) &= 0 \end{aligned} \qquad \text{(A5)}$$

On the planes $w = \pm t$,

$$\begin{aligned} u(x,y,t) - u(x,y,-t) &= 0 \\ v(x,y,t) - v(x,y,-t) &= 0 \\ w(x,y,t) - w(x,y,-t) &= 2w_o \end{aligned} \qquad \text{(A6)}$$

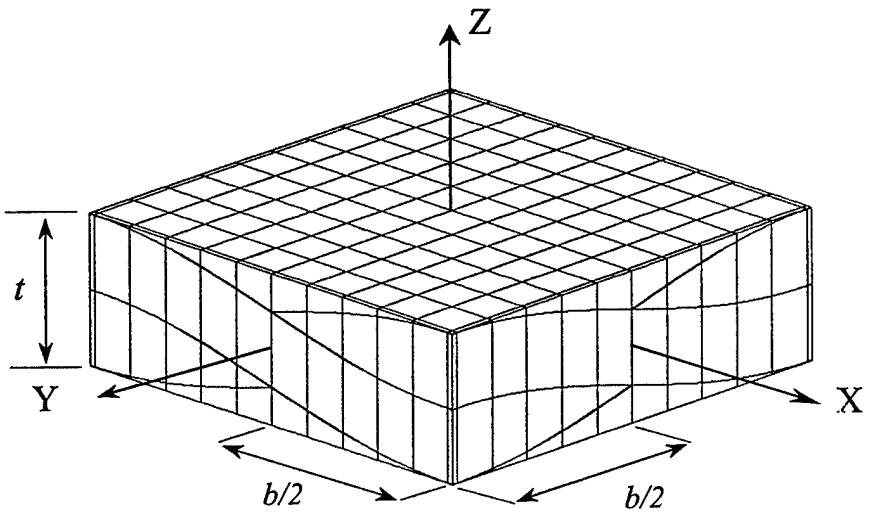

Figure A2. Unit Cell of Plain Weave

Now, for symmetry about the xy, yz, xz planes, the following conditions hold good:

About xy plane:

$$\begin{aligned} u(x,y,z) &= u(x,y,-z) \\ v(x,y,z) &= v(x,y,-z) \\ w(x,y,z) &= -w(x,y,-z) \end{aligned} \qquad \text{(A7)}$$

About the xz plane:

$$\begin{aligned} u(x,y,z) &= u(x,-y,z) \\ v(x,y,z) &= -v(x,-y,z) \\ w(x,y,z) &= w(x,-y,z) \end{aligned} \qquad \text{(A8)}$$

About the yz plane:

$$\begin{aligned} u(x,y,z) &= -u(-x,y,z) \\ v(x,y,z) &= v(-x,y,z) \\ w(x,y,z) &= w(-x,y,z) \end{aligned} \qquad \text{(A9)}$$

Applying these (Eqn. A7-A9) symmetries to Eqn. A4 - A6, the boundary conditions (Figure A2) are:

$$u(\frac{b}{2},y,z) = -u(-\frac{b}{2},y,z) = u_o$$
$$v(x,\frac{b}{2},z) = -v(x,-\frac{b}{2},z) = v_o \qquad \text{(A10)}$$
$$w(x,y,t) = -w(x,y,-t) = w_o$$

A1.1.2 Boundary Conditions for Quarter Cell

The antisymmetry of material distribution about the planes x = 0 and symmetry about the planes x = ± b/2 can be used to derive conditions applicable to each quarter of the unit cell (Figure A3).

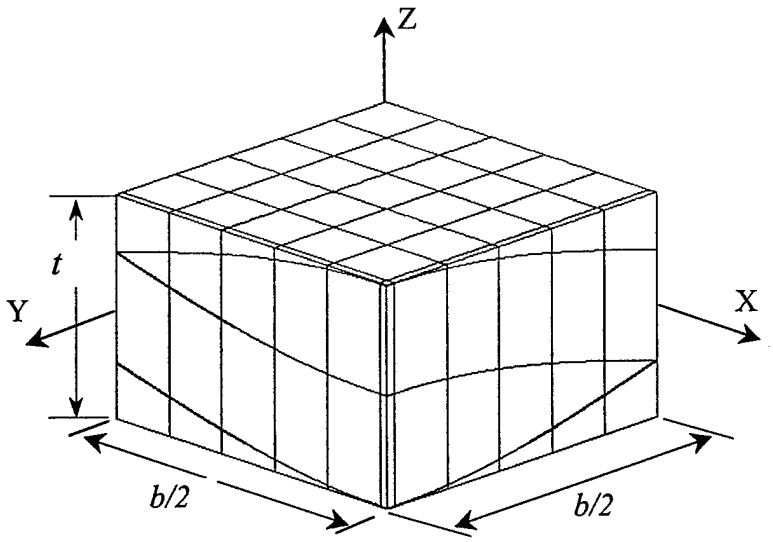

Figure A3. Quarter of Plain Weave Unit Cell

For extension in the x - direction, from the antisymmetry present in the weave, we note that on a x-plane, the following conditions are valid:

$$\text{about the X - axis :} \quad \begin{aligned} u(x,y,z) &= u(x,-y,-z) \\ v(x,y,z) &= -v(x,-y,-z) \\ w(x,y,z) &= -w(x,-y,-z) \end{aligned} \qquad \text{(A11)}$$

Similarly, the anti-symmetric stiffness distribution about the y-axis gives rise to the following conditions:

$$\text{about the Y axis}: \quad \begin{aligned} u(x,y,z) &= -u(-x,y,-z) \\ v(x,y,z) &= v(-x,y,-z) \\ w(x,y,z) &= -w(-x,y,-z) \end{aligned} \tag{A12}$$

Finally, there is point-symmetry about the z-axis. This gives us the relations:

$$\text{about the Z axis}: \quad \begin{aligned} u(x,y,z) &= -u(-x,-y,z) \\ v(x,y,z) &= -v(-x,-y,z) \\ w(x,y,z) &= w(-x,-y,z) \end{aligned} \tag{A13}$$

Eqns. A10-A12 can now be used to obtain the relationship between points lying on the xy, zx and yz planes.

$$\begin{aligned} &\text{on the xy plane}(z=0): && u(x,y,0) = -u(-x,y,0) = u(x,-y,0) \\ &&& v(x,y,0) = v(-x,y,0) = -v(x,-y,0) \\ &&& w(x,y,0) = w(-x,y,0) = -w(x,-y,0) \\ &\text{on the yz plane}(x=0): && u(0,y,z) = -u(0,y,-z) = -u(0,-y,z) \\ &&& v(0,y,z) = v(0,y,-z) = -v(0,-y,z) \\ &&& w(0,y,z) = -w(0,y,-z) = w(0,-y,z) \\ &\text{on the xz plane}(y=0): && u(x,0,z) = -u(-x,0,z) = u(x,0,-z) \\ &&& v(x,0,z) = v(-x,0,z) = -v(x,0,z) \\ &&& w(x,0,z) = w(-x,0,z) = -w(x,0,-z) \end{aligned} \tag{A14}$$

Eqn. A10 specifies the boundary conditions for an *unit cell* with respect to the coordinate axes shown in Figure 1. With respect to a coordinate axes having its origin at the center of the unit cell (in the $x > 0$, $y > 0$ quadrant), we get the boundary conditions for a unit cell subjected to extension as (Figure 2):

$$u(\frac{b}{2},y,z) = -u(-\frac{b}{2},y,z) = \frac{u_o}{2}$$
$$v(x,\frac{b}{2},z) = -v(x,-\frac{b}{2},z) = \frac{v_o}{2} \qquad \text{(A15)}$$
$$w(x,y,\frac{t}{2}) = -w(x,y,-\frac{t}{2}) = \frac{w_o}{2}$$

Eqns A14 and A15 can be used to obtain the boundary conditions for the quarter cell (Figure 3) for the case of in-plane extensional loading in the x direction as :

On the plane $x = 0$:	$u(0,y,z) = -u(0,y,-z)$	
	$v(0,y,z) = v(0,y,-z)$	
	$w(0,y,z) = -w(0,y,-z)$	
Along the $y-$axis $(0,y,0)$:	$u(0,y,0) = 0.0$	
On the plane $y = 0$:	$u(x,0,z) = u(x,0,-z)$	
	$v(x,0,z) = -v(x,0,-z)$	
	$w(x,0,z) = -w(x,0,-z)$	
Along the $x-$axis $(x,0,0)$:	$v(x,0,0) = 0.0$	(A16)
Along the $z-$axis $(0,0,z)$:	$u(0,0,z) = 0$	
	$v(0,0,z) = 0$	
	$w(0,0,z) = -w(0,0,-z)$	
On the plane $x = b/2$:	$u(\frac{b}{2},y,z) = \frac{u_0}{2}$	
On the plane $y = b/2$:	$v(x,\frac{b}{2},z) =$ uniform	

A1.2 BOUNDARY CONDITIONS FOR IN-PLANE SHEAR

A1.2.1 Boundary Conditions for Unit Cell

The periodic cell is subjected to in-plane shear loading using the following conditions:

$$u_A = -u_B = p$$
$$v_A = -v_C = p$$

Substituting the above into Eqn. (A1-A3), we get the following periodic conditions for in-plane shear:

Along the planes $x = \pm b$,

$$\begin{aligned} u(b,y,z) - u(-b,y,z) &= 0 \\ v(b,y,z) - v(-b,y,z) &= 2p \\ w(b,y,z) - w(-b,y,z) &= 0 \end{aligned} \qquad \text{(A17)}$$

Along the planes $y = \pm b$,

$$\begin{aligned} u(x,b,z) - u(x,-b,z) &= 2p \\ v(x,b,z) - v(x,-b,z) &= 0 \\ w(x,b,z) - w(x,-b,z) &= 0 \end{aligned} \qquad \text{(A18)}$$

Along the planes $z = \pm t$,

$$\begin{aligned} u(x,y,t) - u(x,y,-t) &= 0 \\ v(x,y,t) - v(x,y,-t) &= 0 \\ w(x,y,t) - w(x,y,-t) &= 0 \end{aligned} \qquad \text{(A19)}$$

Now, about the xy plane, we have,

$$\begin{aligned} u(x,y,z) &= u(x,y,-z) \\ v(x,y,z) &= v(x,y,-z) \\ w(x,y,z) &= -w(x,y,-z) \end{aligned} \qquad \text{(A20)}$$

About the xz plane,

$$\begin{aligned} u(x,y,z) &= -u(x,-y,z) \\ v(x,y,z) &= v(x,-y,z) \\ w(x,y,z) &= -w(x,-y,z) \end{aligned} \qquad \text{(A21)}$$

About the yz plane,

$$\begin{aligned} u(x,y,z) &= u(-x,y,z) \\ v(x,y,z) &= -v(-x,y,z) \\ w(x,y,z) &= -w(-x,y,z) \end{aligned} \qquad \text{(A22)}$$

Using Eqn. A20, we get

$$w(x,y,0) = 0$$

Also at $z = \pm t$, from Eqn A19 and Eqn. A20 we have

$$w(x,y,t) = w(x,y,-t) = 0$$

From Eqn. A22, at $x = 0$, we get

$$v(0,y,z) = 0$$
$$w(0,y,z) = 0$$

From Eqn A21, at $y = 0$, we get

$$u(x,0,z) = 0$$
$$w(x,0,z) = 0$$

Eqn. A20-A22 together with the periodic conditions, Eqn. A17-A19, yield the following conditions:

$$\begin{aligned} &\text{Eqn A17\&A20} \Rightarrow u(x,b,z) = -u(x,-b,z) = p \\ &\text{Eqn. A16\&A21} \Rightarrow v(b,y,z) = -v(-b,y,z) = p \\ &\text{Eqn.A16\&A21} \Rightarrow \quad w(\pm b,y,z) = 0 \\ &\text{Eqn.A17\&A20} \Rightarrow \quad w(x,\pm b,z) = 0 \\ &\text{Eqn. A18\&A19} \Rightarrow \quad w(x,y,\pm t) = 0 \end{aligned} \qquad \text{(A23)}$$

A1.2.2 Boundary Conditions for Quarter Cell

Boundary conditions for a quarter cell (Figure 3) can now be stated using those of the unit cell. Antisymmetries of loading about the x and y axis give the following relations:

About the x - axis,

$$\begin{aligned} u(x,y,z) &= -u(x,-y,-z) \\ v(x,y,z) &= v(x,-y,-z) \\ w(x,y,z) &= w(x,-y,-z) \end{aligned} \qquad \text{(A24)}$$

About the y - axis,

$$\begin{aligned} u(x,y,z) &= u(-x,y,-z) \\ v(x,y,z) &= -v(-x,y,-z) \\ w(x,y,z) &= w(-x,y,-z) \end{aligned} \qquad \text{(A25)}$$

About the z - axis

$$\begin{aligned} u(x,y,z) &= -u(-x,-y,z) \\ v(x,y,z) &= -v(-x,-y,z) \\ w(x,y,z) &= w(-x,-y,z) \end{aligned} \qquad \text{(A26)}$$

Eqn. (A23) and Eqns. (A24-A26) can be used to obtain the boundary conditions prevalent for the quarter of unit cell shown in Figure A3 as:

$$\begin{aligned} &\text{On the plane } x = 0 \quad u(0,y,z) = u(0,y,-z) \\ &\qquad\qquad\qquad\qquad v(0,y,z) = -v(0,y,-z) \\ &\qquad\qquad\qquad\qquad w(0,y,z) = w(0,y,-z) \\ &\text{On the plane } y = 0 \quad u(x,0,z) = -u(x,0,-z) \\ &\qquad\qquad\qquad\qquad v(x,0,z) = v(x,0,-z) \\ &\qquad\qquad\qquad\qquad w(x,0,z) = w(x,0,-z) \\ &\text{On the plane } y = \frac{b}{2} \qquad u(x,\frac{b}{2},z) = \frac{p}{2} \\ &\qquad\qquad\qquad\qquad w(x,\frac{b}{2},z) = 0 \\ &\text{On the plane } x = \frac{b}{2} \qquad v(\frac{b}{2},y,z) = \frac{p}{2} \\ &\qquad\qquad\qquad\qquad w(\frac{b}{2},y,z) = 0 \end{aligned} \qquad \text{(A27)}$$

APPENDIX B

DAMAGE MECHANICS BASED CONSTITUTIVE LAWS

Suite 250, 500 Office Center Drive
Fort Washington, PA 19034
Tel: 215-542-8400 Fax: 215-542-8401

APPENDIX B – DAMAGE MECHANICS BASED CONSTITUTIVE LAWS

BACKGROUND

Constitutive laws for continuum damage mechanics are discussed in [B1-B3]. Such models have been found to be very successful representing the behavior of brittle materials and make use of a phenomenological approach and the internal variables ω^{α}, which are the damage variables (such as average crack densities). One can write the formulation given in Reference 2 in the following form where $\underline{\sigma}$ and $\underline{\varepsilon}$ are vectors.

$\underline{\sigma} \bullet d\underline{\varepsilon} - \rho d\psi = d\phi \geq 0$; Clausius-Duhem inequality (see Figure A1) (B1a)

ρ = mass density

$\underline{\sigma} = \underline{\sigma}\,[\underline{\varepsilon}, \omega^{\alpha}; \alpha = 1, 2, \ldots k]$

k = total number of damage variables

ψ = Helmholtz free energy

$= \psi\,[\underline{\varepsilon}, \omega^{\alpha}]$

$$\sigma_i = \rho \frac{\partial \psi}{\partial \varepsilon_i} \tag{B1b}$$

$\phi = \phi\,(\underline{\varepsilon}, \omega^{\alpha})$, the dissipated energy density

$$d\phi = \sum_{\alpha=1}^{k} R^{\alpha} d\omega^{\alpha} \geq 0 \tag{B1c}$$

R^{α} = conjugate thermodynamic force, an energy release rate for the damage variable $\omega^{\alpha} = R^{\alpha}\,(\underline{\varepsilon}, \omega^{\alpha})$

$$= -\rho \frac{\partial \psi}{\partial \omega^{\alpha}} = \frac{\partial \phi}{\partial \omega^{\alpha}} \tag{B1d}$$

In the strain energy dissipation (SED) concept employed in [B4], there is one damage variable (k = 1) which is the dissipated energy density ϕ ($=\omega^{1}$), and for this case one may choose the following form for the Helmholtz free energy

$$\rho\psi = \frac{1}{2} C_{ij} \varepsilon_i \varepsilon_j - \int_{0}^{\phi_c} R(\underline{\varepsilon}, \phi) d\phi \tag{B2}$$

where ϕ_c is the current value of ϕ and C_{ij} are the elastic stiffnesses in contracted notation. It follows from the expression for $R^{1} = R$ in (B1d) that for damage growth to occur

$$R(\underline{\varepsilon}, \phi) = 1 \tag{B3}$$

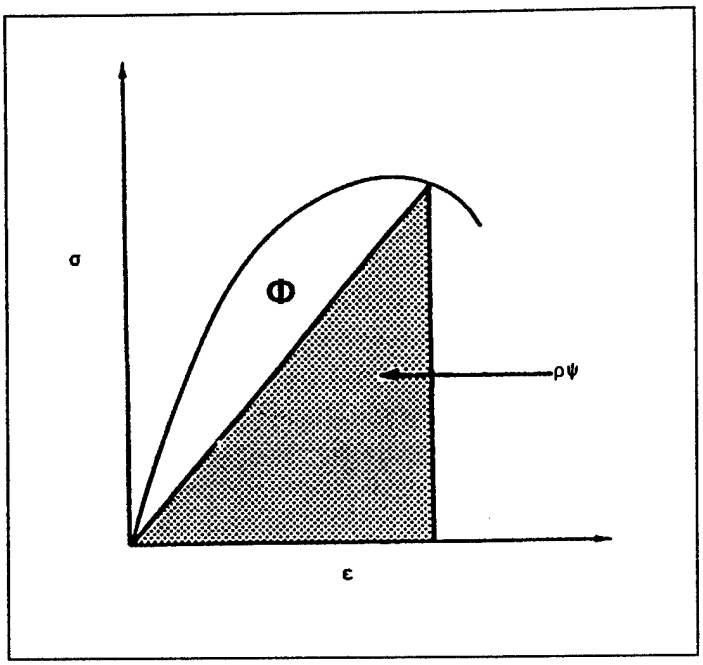

Figure A1. Helmholtz Free Energy $\rho\psi$ and Dissipated Energy ϕ

which defines the damage surface (for a given value of ϕ) in the strain space and when $R(\underline{\varepsilon},\phi) < 1$, no damage growth would occur. It is clear that the dissipated energy is a function of the strain variables independent of the loading path and unloading will occur in a straight line from the current strain state to the origin. Obviously, these assumptions have to be checked by conducting tests and it has been reported that data justify these assumptions. Accordingly, R may be expressed as

$$R(\underline{\varepsilon},\phi) = |\varepsilon|^2 / r^2(\phi,\beta_\gamma) \qquad \text{(B4a)}$$

where for the problem of plane stress (which is addressed in [B4]),

$$|\varepsilon|^2 = \left(\varepsilon_1^2 + \varepsilon_2^2 + \gamma_{12}^2\right) \qquad \text{(B4b)}$$

and r is magnitude of radius vector to the point on the damage surface in the strain space defined by the value of ϕ and two surface coordinates β_γ (γ= 1,2). The subscript 1 refers to the fiber direction, 2 to the transverse direction, and 12 to in-plane shear.

$$\beta_\gamma = \varepsilon_\gamma / |\varepsilon| \quad ; \quad \gamma = 1,2 \qquad \text{(B4c)}$$

In [B4], the damage surfaces (in the three dimensional strain space) are obtained numerically from analysis of data from notched $(\pm\theta)_{ns}$ specimens for various values of θ and different loading paths using a curve fitting procedure. Programmed and controlled loading devices measure the

forces as well as the displacements at the loading points, so that the total energy dissipation in the specimens can be computed. Finite element analysis and computed elastic strain fields in the specimen are utilized for analysis of data.

Authors of [B4] plan to make their analysis methodology available through the world wide web, but currently neither the method nor the data (damage surfaces) are available for use. For nonlinear stress analysis of laminated plates with and without stress raisers (holes or cracks), the following simple form of the damage surfaces was employed in [B5, B6].

$$\begin{aligned} R(\varepsilon_i,\phi) = \frac{1}{2}\Big[&\{a_{11}(\phi)+b_{11}(\phi)\operatorname{sgn}\varepsilon_1\}\varepsilon_1^2 \\ &+\{a_{22}(\phi)+b_{22}(\phi)\operatorname{sgn}\varepsilon_2\}\varepsilon_2^2 \\ &+2a_{12}(\phi)\varepsilon_1\varepsilon_2+a_{66}(\phi)\gamma_{12}^2\Big] \\ =1& \end{aligned} \qquad \text{(B5a)}$$

It may be noted that (B5a) is a Tsai-Wu type quadratic failure criterion in terms of strain (with different coefficients in the four quadrants of $\varepsilon_1\varepsilon_2$ plane and no linear terms). The coefficients $(a_{11}\pm b_{11})$, $(a_{22}\pm b_{22})$, a_{12} and a_{33} are functions of ϕ and they may vary with ϕ in different fashions, but subsequent damage surfaces must enclose the previous ones. Based on the results of studies on failure theories of unidirectional composites, it appears that the representation of the damage surfaces by (B5a) may not be very accurate for small values of ϕ, but it provides a reasonable estimate of stiffness losses. As discussed later, the representation is quite good for moderate to high values of ϕ.

The residual stiffnesses of Q_{ij}^* after some energy dissipation obtained using the constitutive law are given below. Note that C_{ij} in (B2) must be replaced by Q_{ij} (reduced stiffnesses for plane stress problems).

$$\begin{aligned} Q_{11}^* &= Q_{11}-(A_{11}(\phi)+B_{11}(\phi)\operatorname{sgn}\varepsilon_1) \\ Q_{22}^* &= Q_{22}-(A_{22}(\phi)+B_{22}(\phi)\operatorname{sgn}\varepsilon_2) \\ Q_{12}^* &= Q_{12}-A_{12}(\phi) \\ Q_{66}^* &= Q_{66}-A_{66}(\phi) \end{aligned} \qquad \text{(B5b-d)}$$

where

$$\left[A_{ij}(\phi),B_{ij}(\phi)\right]=\int_0^{\phi}\left[a_{ij}(\phi),b_{ij}(\phi)\right]d\phi \qquad \text{(B5e)}$$

It may be noted that (a_{ij},b_{ij}) or (A_{ij},B_{ij}) can be determined if stress-strain responses are known from displacement controlled tests with unidirectional straining. For example, A_{66} (or a_{66})

will be known from the nonlinear shear stress-strain curve for the unidirectional composite. However, unidirectional straining is difficult to conduct and sudden failures may often occur in testing unidirectional materials. To obtain a better representation of the in-situ behavior of a lamina in a laminate, test data from laminate tests are preferable for determination of the coefficients a_{ij} and b_{ij} as functions of ϕ. Tension and compression test data of $(\pm\theta)_{ns}$ laminates (θ=30,45°,60°) were utilized in [B5] to estimate a_{22}, b_{22}, and a_{66} since stiffness losses in the fiber direction (reduction in Q_{11}) are very small in these laminate tests.

Determination of a_{11} and b_{11} (or axial stiffness losses) is a more difficult problem, because standard tension or compression tests on laminates ($(0/90)_{ns}$ or $(0/\pm45/90)_{ns}$) show very little nonlinear response up to the maximum load at which sudden failure occurs. The Poisson strain in $(0/90)_{ns}$ laminates show some nonlinear response from which a_{12} was estimated. It should be noted that for high modulus carbon/epoxy composites (such as AS4/3501-6), the transverse (extensional) and shear stiffnesses Q_{22} and Q_{66} are small compared to the axial stiffness Q_{11} and damage initiation strain ε_2 (or γ_{12}) is usually smaller than (or of the same order as) that in the fiber direction (ε_1). For this reason, the energy to be dissipated for complete loss in transverse (or shear) stiffness is much smaller (of the order of 150-300 in lb/in^3) than that required to cause complete loss in fiber direction stiffness (of the order of 5000-7000 in lb/in^3). Displacement controlled tests on $(0/90)_{ns}$ or $(0/\pm45/90)_{ns}$ laminates are very difficult to conduct and, therefore, it appears that the best approach to estimate a_{11}, b_{11} will be to conduct tests on laminates with holes or notches, and then correlate the results with those from appropriate stress (strain) analyses using various chosen values of $a_{11}(\phi), b_{11}(\phi)$. Matching the local response (load vs. notch opening displacement or notch tip strain) will yield the desired coefficients. Calculations [B5] show that it is possible to do so and the results also explain the so-called "hole size effect" observed in tests. It may be noted that at high values of ϕ (>300 in lb/in^3), all the coefficients in (B5a) except a_{11} and b_{11} and all the stiffnesses in (B5b-d) except Q^*_{11} approach zero, but the loss in fiber direction stiffness continues (initially at a fast rate and then at a slower rate) up to very high values of ε_1 (> 5%), which indicates that a lot of energy is dissipated through a process of progressive fiber breaks (kinks) followed or accompanied by gradual fiber pull out or other similar processes. Therefore, for large values of ϕ, the damage surfaces can be described in terms of ε_1 alone. In many problems of practical interest, it may not be necessary to model the material response up to such high values of dissipated energy density, but the roles played by interlaminar strains and stresses may be quite significant. Responses of textile composites are ob-

viously influenced by such stresses and strains and it is, therefore, necessary to obtain a representation of $R(\underline{\varepsilon},\phi)$ including the effects of interlaminar strains. Such representations are presented in the next section. It should be noted that for obvious reasons, no influence of laminate stacking order is predicted by the model discussed above [B5] for the "hole size effect" problem, and the representations given next should also be useful for estimating the influence of stacking in such problems.

DAMAGE SURFACES FOR A TRANSVERSELY ISOTROPIC COMPOSITE

The problem of plane stress addressed in the previous section is an approximation. It may be noted that when the through the thickness stress σ_3 is zero, it is highly unlikely that the corresponding strain component in the damaged state is related to the other two strains ε_1 and ε_2 via the elastic relation, i.e., the sum of the two products obtained by multiplying these strains with the appropriate Poisson's ratios. Such a relation is not consistent since the use of the reduced stiffnesses in (B5b) imply that when σ_2 is zero, $\varepsilon_2 = -Q^*_{12}\varepsilon_1 / Q^*_{22}$, which may not necessarily be the same in the elastic domain. Experiences in the use of the theory of plasticity indicates that inconsistencies may arise if a plasticity theory is formulated by choosing some of the stress components as zero. Therefore, it appears necessary to obtain a constitutive law retaining all the strain and stress components. For a fiber composite which is transversely isotropic in the elastic state, one can write the Helmholtz free energy in the following form.

$$\rho\psi = \frac{1}{2}\Big[C_{11}\varepsilon_1^2 + 2C_{12}\varepsilon_1\varepsilon_s + k\varepsilon_s^2 + G_T\left(\varepsilon_d^2 + \gamma_{23}^2\right) + G_A\left(\gamma_{12}^2 + \gamma_{13}^2\right)\Big] - \int_0^{\phi} R(\underline{\varepsilon},\phi)\,d\phi \qquad \text{(B6a)}$$

where

$$\varepsilon_s = \varepsilon_2 + \varepsilon_3 \qquad \text{(B6b,c)}$$
$$\varepsilon_d = \varepsilon_2 - \varepsilon_3$$

k is the plane strain bulk modulus and G_A and G_T are the axial and transverse shear moduli, respectively. The stresses are given by

$$\sigma_1 = \frac{\partial(\rho\psi)}{\partial\varepsilon_1}$$
$$\frac{\sigma_2 + \sigma_3}{2} = \frac{\partial(\rho\psi)}{\partial\varepsilon_s}$$
$$\frac{\sigma_2 - \sigma_3}{2} = \frac{\partial(\rho\psi)}{\partial\varepsilon_d} \qquad \text{(B6d-i)}$$
$$\tau_{12} = \frac{\partial(\rho\psi)}{\partial\gamma_{12}}$$
$$\tau_{13} = \frac{\partial(\rho\psi)}{\partial\gamma_{13}}$$
$$\tau_{23} = \frac{\partial(\rho\psi)}{\partial\gamma_{23}}$$

Based on the assumption of a quadratic interaction criterion in terms of stresses, one may choose the following form of R for zero (damage initiation) to small values of the dissipated energy density

$$\begin{aligned} R(\underline{\varepsilon},\phi) = \frac{1}{2}\Big[&\left\{a_{11}(\phi)+b_{11}(\phi)\operatorname{sgn}\varepsilon_1^*\right\}\varepsilon_1^{*2} \\ &+\left\{a_{22}(\phi)+b_{22}(\phi)\operatorname{sgn}\varepsilon_s^*\right\}\varepsilon_s^{*2} \\ &+a_{44}(\phi)\left(\varepsilon_d^2+\gamma_{23}^2\right)+a_{66}(\phi)\left(\gamma_{12}^2+\gamma_{13}^2\right)\Big] \end{aligned} \tag{B7a}$$

where

$$\begin{aligned} \varepsilon_1^* &= \varepsilon_1+\alpha_{12}\varepsilon_s \\ \varepsilon_s^* &= \varepsilon_s+\alpha_{21}\varepsilon_1 \\ \alpha_{12} &= C_{12}/C_{11} \\ \alpha_{21} &= C_{12}/k \end{aligned} \tag{B7b-e}$$

Use of (B6a-i) yields a transversely isotropic material with the following values of reduced stiffnesses in the damaged state for the current value of ϕ.

$$\begin{aligned} C_{11}^* &= C_{11}-\left(A_{11}(\phi)+B_{11}(\phi)\operatorname{sgn}\varepsilon_1^*\right)-\left(A_{22}(\phi)+B_{22}(\phi)\operatorname{sgn}\varepsilon_s^*\right)\alpha_{21}^2 \\ C_{12}^* &= C_{12}-\left(A_{11}(\phi)+B_{11}(\phi)\operatorname{sgn}\varepsilon_1^*\right)\alpha_{12}-\left(A_{22}(\phi)+B_{22}(\phi)\operatorname{sgn}\varepsilon_s^*\right)\alpha_{21} \\ k^* &= k-\left(A_{22}(\phi)+B_{22}(\phi)\operatorname{sgn}\varepsilon_s^*\right)-\left(A_{11}(\phi)+B_{11}(\phi)\operatorname{sgn}\varepsilon_1^*\right)\alpha_{12}^2 \\ C_{44}^* &= G_T-A_{44}(\phi) \\ C_{66}^* &= G_A-A_{66}(\phi) \end{aligned} \tag{B7f-j}$$

where

$$\left[A_{ij}(\phi),B_{ij}(\phi)\right]=\int_0^\phi\left(a_{ij}(\phi),b_{ij}(\phi)\right)d\phi \tag{B7k}$$

Representations, which are more complicated than (B7a), may have to be chosen to match test data if they indicate that the damaged composite behaves as an orthotropic or a more highly anisotropic (one case is discussed later) material. It is worthwhile, however, to examine whether the simple representation can yield reasonable correlation for small values of ϕ. Further simplification can be achieved by choosing

$$\begin{aligned} b_{22}(\phi) &= a_{22}(\phi) \\ B_{22}(\phi) &= A_{22}(\phi) \end{aligned} \tag{B7l,m}$$

which imply that hydrostatic compression in the plane of transverse isotropy does not cause any damage, or in other words, damage may occur only at very high values of hydrostatic compressive strain, which is not of interest in problems of the type under consideration [B7, B8]. Further, for small to moderate values of ϕ, it is possible to use the following representations for the

losses in various stiffnesses in (B7f-k) and (B7m) to match test data for softening observed in $(\pm\theta)_{ns}$ and other layups.

$$A_{11}(\phi) \pm B_{11}(\phi) = C_{11}\left[1-\left(1+\phi/\phi_1^{\pm}\right)^{-n_1^{\pm}}\right]$$

$$2A_{22}(\phi) = A_{22}(\phi) + B_{22}(\phi) = k\left[1-\left(1+\phi/\phi_2^{+}\right)^{-n_2^{+}}\right] \qquad \text{(B8a-d)}$$

$$A_{44}(\phi) = G_T\left[1-\left(1+\phi/\phi_4\right)^{-n_4}\right]$$

$$A_{66}(\phi) = G_A\left[1-\left(1+\phi/\phi_6\right)^{-n_6}\right]$$

It may be noted that these representations are adequate when the stress-strain relations are of the power law type after the onset of damage. For example, if the axial shear stress-strain relation is of the following form ($\tau_{12}^0, \gamma_{12}^0$ being the stress and strain at damage onset)

$$\tau_{12} = \tau_{12}^0\left(\gamma_{12}/\gamma_{12}^0\right)^{\lambda_6} \qquad \text{(B8e)}$$

then n_6 and ϕ_6 are given by

$$n_6 = 2/(\lambda_6+1) - 1$$

$$\phi_6 = G_A \gamma_{12}^{0^2} n_6/2 \qquad \text{(B8f,g)}$$

From test data for AS4/3501-6 laminates reported in literature and fits performed in [B5] (where $a_{ij}(\phi), b_{ij}(\phi), A_{ij}(\phi), B_{ij}(\phi)$, etc., were chosen by linear interpolation in ϕ from tabulated values), it appears that the following parameters should yield reasonable fits to the laminate responses when ϕ is not large.

$$\begin{aligned}
n_1^+ &= 2.576, & \phi_1^+ &= 4812 \text{ in lb/in}^3 \\
n_1^- &= 1.372, & \phi_1^- &= 2810 \text{ in lb/in}^3 \\
n_2^+ &= 2.538, & \phi_2^+ &= 22.68 \text{ in lb/in}^3 \\
n_4 &= 0.287, & \phi_4 &= 11.40 \text{ in lb/in}^3 \\
n_6 &= 0.478, & \phi_6 &= 14.86 \text{ in lb/in}^3
\end{aligned} \qquad \text{(B9a-e)}$$

Representations of the types described in the sets of equations (B7, A8) are currently being used for problems with small to moderate stiffness losses in some textile composites.

Power law type representations with constant values of the indices n_i may not be always adequate, especially for larger values of ϕ. Better representations can, however, be obtained by choosing the indices n_i as functions of ϕ. For example, one may choose

$$A_{11}(\phi) \pm B_{11}(\phi) = C_{11}\left[1-\left(1-\phi/\phi_1^{\pm}\right)^{-n_1^{\pm}(\phi/\phi_1^{\pm})}\right] \qquad \text{(B10)}$$

instead of (B9a) and similar relations for the quantities in (B9b-d). Differentiation of equations of the type (B10) yields the coefficients $a_{ij}(\phi), b_{ij}(\phi)$. For example, from (B10) one can obtain

$$a_{ij}(\phi) \pm b_{ij}(\phi) = \frac{C_{11} n_1^{\pm}}{\phi_1^{\pm}} \left(1 + \phi / \phi_1^{\pm}\right)^{-(n_1^{\pm}+1)} \left\{1 + \frac{n_1^{\pm'}}{n_1^{\pm}} \left(1 + \phi / \phi_1^{\pm}\right) \ln\left(1 + \phi / \phi_1^{\pm}\right)\right\} \tag{B11}$$

where

$$n_1^{\pm'} = \frac{dn_1^{\pm}}{d\left(\phi / \phi_1^{\pm}\right)} \tag{B12}$$

Although representations of the type discussed here should be adequate, when n_i are weak functions of ϕ, it is necessary to check that the damage surfaces for any value of $\phi = \phi^*$ enclose the ones for values of $\phi < \phi^*$.

It was pointed out in the last section that for large values of ϕ, the damage surfaces can be described by ε_1 alone, since matrix dominated stiffnesses reduce to negligible values for moderate values of ϕ, but fiber direction stiffnesses reduce at a slower rate as straining continues. Because of this behavior, one should expect that α_{12} chosen in (B7a,b) as a constant should change with ϕ reducing to zero for moderately large values of ϕ. One should note, however, that values of $\alpha_{12} = C_{12} / C_{11}$ for high modulus fiber composites are usually small and hence a modified and integrated version of (B7a) given below may be better suited for modeling the behavior almost to the point of complete stiffness loss. The integrated form is useful when n_i are functions of ϕ (as in (B10-A12)).

$$\begin{aligned} \int_0^{\phi} R(\underline{\varepsilon}, \phi) d\phi = \frac{1}{2} \Big[& \left(A_{11}(\phi) + B_{11} \operatorname{sgn} \varepsilon_1\right) \varepsilon_1^2 \\ & + \left(A_{22}(\phi) + B_{22} \operatorname{sgn} \varepsilon_s^*\right) \varepsilon_s^{*2} \\ & + A_{44}(\phi)\left(\varepsilon_d^2 + \gamma_{23}^2\right) + A_{66}(\phi)\left(\gamma_{12}^2 + \gamma_{13}^2\right) \Big] \end{aligned} \tag{B13a}$$

It may be noted that if ε_1 is replaced by ε_1^* and (B13a) is differentiated with respect to ϕ one obtains (B7a). Since α_{12} is small, results obtained using (B13a) should not differ significantly from those using (B7a) for small stiffness losses. It should also be noted that the choices (B7l, m) will not be suitable for large values of ϕ, since stiffness loss would be expected under in-plane hydrostatic compression at large strain levels. Therefore, one additional coefficient must be chosen by matching data from tests under appropriate strain states/paths. Use of (B13a) and (B6a-i) yields reduced stiffnesses in the forms (B7f-j) with the following changes in (B7f-h).

$$C_{11}^{*} = C_{11} - \left(A_{11}(\phi) + B_{11}(\phi)\operatorname{sgn}\varepsilon_1\right) - \left(A_{22} + B_{22}\operatorname{sgn}\varepsilon_s^{*}\right)\alpha_{21}^2$$

$$C_{12}^{*} = C_{12} - \left(A_{22} + B_{22}\operatorname{sgn}\varepsilon_s^{*}\right)\alpha_{21} \qquad \text{(B13b-d)}$$

$$k^{*} = k - \left(A_{22} + B_{22}\operatorname{sgn}\varepsilon_s^{*}\right)$$

If one wishes to simulate states approaching complete stiffness loss (for large values of ϕ), one may choose the following representations instead of (B8a,b).

$$A_{11}(\phi) \pm B_{11}(\phi) = \left(C_{11} - C_{12}^2/k\right)\left[1 - \left(1 + \phi/\phi_1^{\pm}\right)^{-n_1^{\pm}}\right]$$

$$A_{22}(\phi) \pm B_{22}(\phi) = k\left[1 - \left(1 + \phi/\phi_2^{\pm}\right)^{-n_2^{\pm}}\right] \qquad \text{(B13e,f)}$$

$A_{44}(\phi), A_{66}(\phi)$ can be chosen to be the same as (B8c,d). The indices $n_i^{\pm}$ may be assumed to be weak functions of ϕ as discussed earlier.

Finally, one should note that the representation (B13a) involving squares of the strain variables and those of the types (B10-A12) are still very simple and may not be adequate in some cases. One phenomenon, which may need some consideration, is the effect of in-plane hydrostatic strain (or stress) on damage in a state dominated by shear. Experimental data indicate that shear strains (or stresses) to cause initial (and progressive) damage are usually increased when hydrostatic compression [B7, B8] is present. Such behavior can possibly be modeled by choosing the following modified form of (B13a).

$$\begin{aligned}\int_o^{\phi} R(\underline{\varepsilon},\phi)\,d\phi = \frac{1}{2}\Big[&\left(A_{11}(\phi) + B_{11}\operatorname{sgn}\varepsilon_1\right)\varepsilon_1^2 \\ &+ \left(A_{22}(\phi) + B_{22}\operatorname{sgn}\varepsilon_s^{*}\right)\varepsilon_s^{*2} \\ &+ A_{44}(\phi)\left(\varepsilon_d^2 + \gamma_{23}^2\right)\left(1 + \delta_1(\phi)\cos\theta_1\right) \\ &+ A_{66}(\phi)\left(\gamma_{12}^2 + \gamma_{13}^2\right)\left(1 + \delta_2(\phi)\cos\theta_2\right)\Big]\end{aligned} \qquad \text{(B14a)}$$

where

$$\tan\theta_1 = \left(\varepsilon_d^2 + \gamma_{23}^2\right)^{1/2}/\varepsilon_s^{*} \qquad \text{(B14b)}$$

$$\tan\theta_2 = \left(\gamma_{12}^2 + \gamma_{13}^2\right)^{1/2}/\varepsilon_s^{*} \qquad \text{(B14c)}$$

and $\delta_1(\phi), \delta_2(\phi)$ are functions of ϕ to be chosen to match test data. It is expected that δ_1 and δ_2 should approach zero for large ϕ and accordingly they may be chosen as

$$\delta_1(\phi) = \delta_{10}\left(1 + \phi/\phi_4\right)^{-n_7(\phi)} \qquad \text{(B14d)}$$

$$\delta_2(\phi) = \delta_{20}\left(1 + \phi/\phi_6\right)^{-n_8(\phi)} \qquad \text{(B14e)}$$

δ_{10} and δ_{20} may be selected based on available data for initial damage following procedures similar to those used in [B8]. n_7 and n_8 may be chosen if subsequent damage surfaces under combined shear and hydrostatic in-plane compression and tension can be estimated from test data. As initial estimates n_7 and n_8 may be chosen equal to n_4 and n_6, respectively. It may be noted that evaluation of stresses using the representations (B14a-e) and the relations (B6d-i) indicates that the stress total strain relations in the damaged state are complicated and the stiffness matrix (reduced) is no longer symmetric. This is a result of the complex but more realistic damage surfaces chosen (B14a) and has been discussed in [B4]. This complexity also necessitates the examination of the damage surfaces, so as to ensure that the present one encloses the previous surfaces.

DAMAGE SURFACES FOR AN ISOTROPIC MATERIAL

In addition to the unidirectional fiber composites in wavy forms, textile composites contain matrix pockets, which are also brittle and will undergo stiffness loss with increasing strain. The Helmholtz free energy for such materials can be expressed in the following form based on the principles of damage mechanics and assumptions similar to those used for the damage surfaces (in the previous section) for fiber composites.

$$\rho\psi = \tfrac{1}{2}\left[K\varepsilon_v^2 + G\gamma_{eff}^2\right] - \int_0^{\phi} R(\underline{\varepsilon},\phi)d\phi$$
$$\gamma_{eff}^2 = 2\left(\varepsilon_{11}'^2 + \varepsilon_{22}'^2 + \varepsilon_{33}'^2\right) + \gamma_{12}^2 + \gamma_{23}^2 + \gamma_{13}^2 \qquad \text{(B15a,b)}$$

where K is the bulk modulus, G is the shear modulus.

$$\varepsilon_v = \varepsilon_{11} + \varepsilon_{22} + \varepsilon_{33}, \text{ volumetric strain}$$
$$\varepsilon_{ij}' = \varepsilon_{ij} - \varepsilon_v/3; (i = j), \text{ deviatoric strains} \qquad \text{(B15c-e)}$$
$$\gamma_{ij} = \text{shear strains}; (i \neq j)$$

$$R(\underline{\varepsilon},\phi) = 1 \text{ (for damage growth to occur)} \qquad \text{(B15f)}$$

(B15f) define the damage surfaces for various values of ϕ and no damage growth will occur if $R(\underline{\varepsilon},\phi) < 1$.

The stresses are given by

$$\sigma_m = (\sigma_{11} + \sigma_{22} + \sigma_{33})/3 = \frac{\partial(\rho\psi)}{\partial\varepsilon_v}, \text{ mean stress}$$

$$\sigma_{ij}' = \sigma_{ij} - \sigma_m = \frac{\partial(\rho\psi)}{\partial\varepsilon_{ij}'}; (i = j), \text{ deviatoric stresses} \qquad \text{(B15g-i)}$$

$$\tau_{ij} = \frac{\partial(\rho\psi)}{\partial\gamma_{ij}}; (i \neq j), \text{ shear stresses}$$

The simplest form of $R(\underline{\varepsilon},\phi)$, which may be chosen is of the following forms

$$R(\underline{\varepsilon},\phi) = \frac{1}{2}\left[(a_v(\phi) + b_v(\phi)\operatorname{sgn}\varepsilon_v)\varepsilon_v^2 + a_s(\phi)\gamma_{eff}^2\right.$$
$$\left.\int_0^{\phi} R(\varepsilon,\phi)d\phi = \frac{1}{2}\left[(A_v(\phi) + B_v(\phi)\operatorname{sgn}\varepsilon_v)\varepsilon_v^2 + A_s(\phi)\gamma_{eff}^2\right]\right. \qquad \text{(B16a,b)}$$

Substitution of (B16b) in (B15a) and use of (B15g-i) yield the following expressions for stresses

$$\sigma_{ij} = \left\{K - (A_v(\phi) + B_v(\phi)\operatorname{sgn}\varepsilon_v) - \frac{2}{3}(G - A_s(\phi))\right\}\varepsilon_v\delta_{ij}$$
$$+ 2(G - A_s(\phi))\varepsilon_{ij}; i = j \qquad \text{(B16c,d)}$$
$$\tau_{ij} = \{G - A_s(\phi)\}\gamma_{ij}; i \neq j$$

It is clear that the damaged material behaves as an isotropic material with a reduced bulk modulus of $\{K-(A_v(\phi)\pm B_v(\phi)\}$ and a reduced shear modulus of $\{G-A_s(\phi)\}$. More complicated representations can be chosen, if desired, for the purpose of matching test data for various strain paths and strain ranges, but it appears worthwhile to examine the usefulness and range of validity of the simple representations. Additional simplifying assumption may be made by neglecting the effect of hydrostatic compression (valid over a limited range of strains) and choosing

$$b_v(\phi)=a_v(\phi)$$
$$B_v(\phi)=A_v(\phi) \qquad \text{(B16e,f)}$$

Based on power law type representation of stress-strain relations (discussed for composites in the previous section) beyond the elastic region, one may also choose

$$2A_v(\phi)=A_v(\phi)+B_v(\phi)=K\left[1+\left(\phi/\phi_v^+\right)^{-n_v^+}\right]$$
$$A_s(\phi)=G\left[1-\left(1+\phi/\phi_s\right)^{-n_s}\right] \qquad \text{(B17a,b)}$$

with n_v and n_s chosen as constants (for low to moderate values of ϕ) or as weak functions of ϕ (for wider range of strains and ϕ). In the latter case, however, effect of hydrostatic compression may have to be considered (assumptions (B16e,f) may not be valid) and it would be necessary to introduce additional parameters, i.e.,

$$A_V(\phi)\pm B_v(\phi)=K\left[1-\left(1+\frac{\phi}{\phi_v^{\pm}}\right)^{-n_v^{\pm}}\right] \qquad \text{(B18)}$$

Finally, the increase in shear strains (or stresses) to cause damage with increase in hydrostatic compressive strain (or stresses) can be modeled by the following modification

$$\int_0^{\phi} R(\varepsilon,\phi)d\phi=\frac{1}{2}\Big[\left(A_v(\phi)+B_v(\phi)\operatorname{sgn}\varepsilon_v\right)\varepsilon_v^2$$
$$+A_s(\phi)\gamma_{eff}^2\left(1+\delta_v\cos\theta\right)\Big] \qquad \text{(B19)}$$

where

$$\tan\theta=\frac{\gamma_{eff}}{\varepsilon_v} \qquad \text{(B20)}$$

and δ_v (a constant or a function of ϕ) has to be chosen to match experimental results similar to those used to select the parameters in Mohr-Coulomb type failure theories (see, for example, [B8]). The resulting stress-total strain relations are complicated and the stiffness matrix may not be symmetric as discussed in the previous section.

REFERENCES

B1. Krajcinovic, D., "Continuous Damage Mechanics Revisited" Basic Concepts and Definitions", ASME J. Appl. Mech., Vol. 52., p. 829, 1985.

B2. Illankamban, R., and Krajcinovic, D., "A Constitutive Theory for Progressively Deteriorating Solids", International Journal of Solids and Structures, Vol. 23, p. 1521, 1987.

B3. Chaboche, J.L., "Continuum Damage Mechanics, Parts I and II", ASME J. Applied Mechanics, Vol. 55, p. 59 and p. 65, 1989.

B4. Mast, P.W. et al., "Characterization of Strain-Induced Damage in Composites Based on the Dissipated Energy Density, Parts I-III", Theoretical and Applied Fracture Mechanics, Vol. 22, p. 71, p. 97, p. 115, 1995.

B5. Chatterjee, S.N., and Yen, C.F., "Energy Dissipation Characterization and Design Methodology for Composite Materials", MSC TFR 3610/AA20, NASC Contract No. N0019-96-C-2028, November 1996.

B6. Chatterjee, S.N., Yen, C.-F., and Mirto, D., "Failure and Damage Tolerance of Composite Materials", MSC TFR 3712/BD01, NAS1-97053, September. 1997.

B7. Hashin, Z., "Failure Criteria for Unidirectional Fiber Composites", ASME J. Appl. Mech., Vol. 47, p. 329, 1980.

B8. Chatterjee, S.N., " A Coulomb-Mohr Type Criterion for Matrix Mode Failure in a Lamina", in Composite Materials: testing and Design, 13th Vol., S.J. Hooper, Editor, ASTM STP 1242, ASTM, West Conshohocken, PA, October 1997.

APPENDIX C

THERMO-MECHANICAL PROPERTIES OF A REPRESENTATIVE AREA ELEMENT

Suite 250, 500 Office Center Drive
Fort Washington, PA 19034
Tel: 215-542-8400 Fax: 215-542-8401

25 Years Advanced Composites Technology

APPENDIX C – THERMO-MECHANICAL PROPERTIES OF A REPRESENTATIVE AREA ELEMENT

SUMMARY

This Appendix examines fundamental micromechanical relations, and how they may be generalized to cover a wider class of material forms. In particular, the typical homogenization process applied to multiphase materials has been modified into a form more amenable to textile composites. This approach supports a goal of obtaining useful results using analytic, closed-form methods. The methodology can also be supported by finite element, and other numerical methods. But the numerical methods must be supported by strong, fundamental mechanics.

INTRODUCTION

Laminated composite plates containing layers of unidirectionally reinforced continuous fiber composites of various orientations are now being widely used for various structural applications. The state-of-the-art of evaluating their structural performance is quite advanced and their mechanical behavior is well defined. On the other hand, the mechanics of woven fabric reinforced composite plates, manufactured by combining the age old technology of textiles and processing methods recently developed for laminated fiber composite plates, are still not clearly understood. Several attempts have been made to characterize the structural response of such plates based on various geometric parameters and properties of the constituent fiber and matrix materials (for a survey, see [C1]). The main idea behind these studies is to use the concept of equivalent homogeneity, widely used in mechanics of fiber reinforced composites [C2]. These methods attempt to find the relationship between either average stresses and average strains or average stress resultants and average mid-plane strains and plate curvatures. We first consider the definitions of these average quantities and give some simple theorems relating them to displacements and tractions. The displacements and/or tractions are applied on the boundary of a representative area element (Figure C1), which consists of several nonhomogeneous layers. Each layer is either a homogeneous material (such matrix layers are often used in practice) or a fabric reinforced composite. Each fabric reinforced layer can be further divided into a number of sublayers, if needed. It is assumed that each layer (or sublayer) consists of a finite number of materials (unidirectionally or bidirectionally reinforced composite or matrix material), whose thermomechanical properties are known. For calculating the thermomechanical

response of the RAE ways to obtain simple bounds on the effective plate properties, as well as other approaches are suggested.

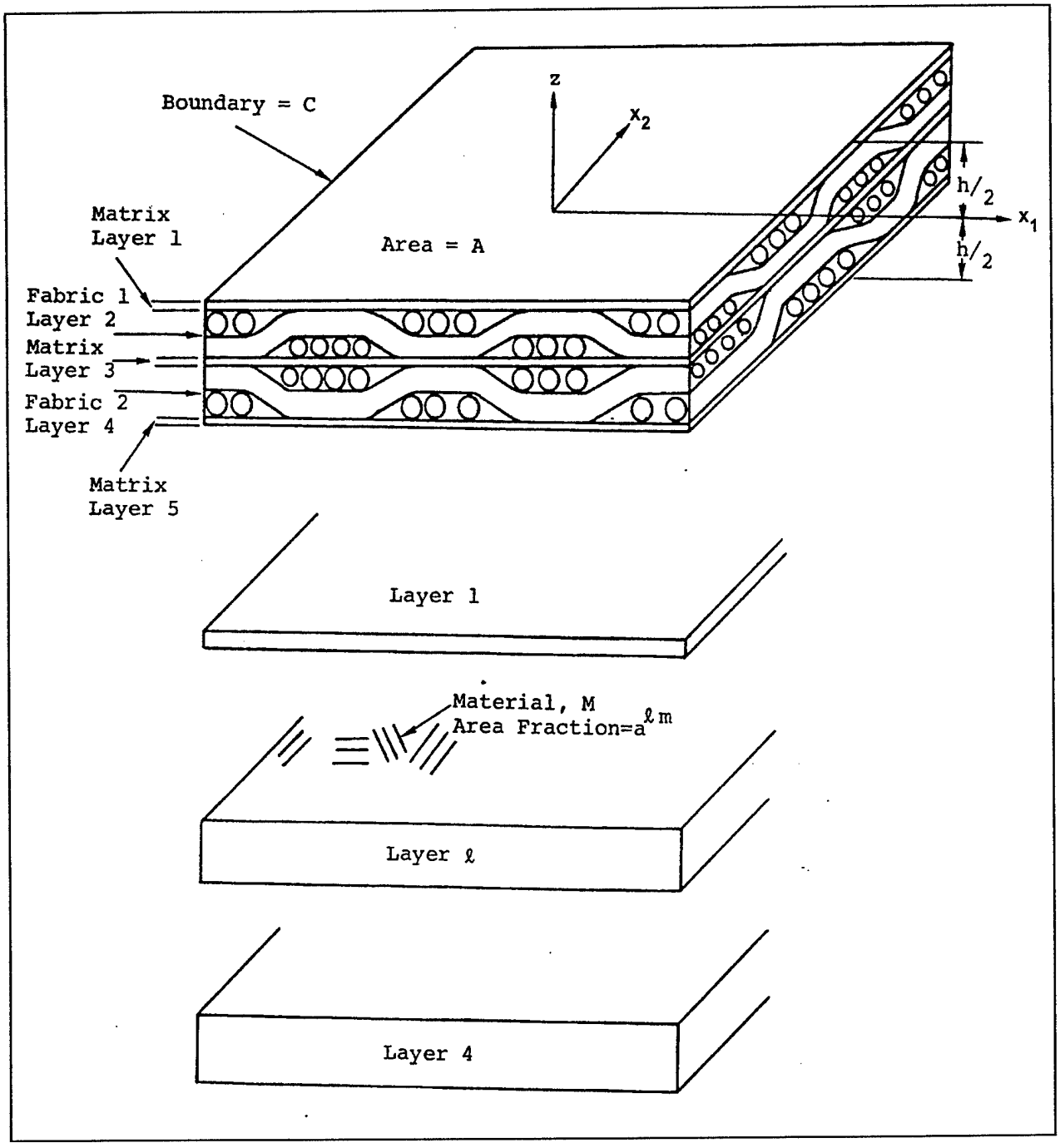

Figure C1. Representative Area Element (RAE) Containing Several Layers

DEFINITIONS AND THEOREMS

Average Displacements and Forces

We define the average mid-plane strains, curvatures and transverse shear strains in the following manner:

$$\bar{\varepsilon}_{ij} = \frac{1}{2hA}\int_A \int_{-h/2}^{h/2} \left(u_{i,j} + u_{j,i}\right) dz\, dA$$
$$\bar{\kappa}_{ij} = \frac{6}{h^3 A}\int_A \int_{-h/2}^{h/2} \left(u_{i,j} + u_{j,i}\right) z\, dz\, dA \qquad ; i,j = 1,2 \qquad (C1)$$
$$\bar{\gamma}_{i3} = 2\bar{\varepsilon}_{i3} = \frac{1}{hA}\int_A \int_{-h/2}^{h/2} \left(u_{i,3} + u_{3,i}\right) dz\, dA$$

where h is thickness of the plate and A is the area of representative element (RAE). An example is shown in Figure C1. u_1, u_2 are the displacements in x and y directions which, in general, depend on the space variables x, y and z. Obviously, the size of the RAE should be large compared to the "mini" structural dimensions to make the averaging process meaningful [C1]. If these quantities are to be used for determining the plate response in practical applications, the size of the structural plate element should be sufficiently large as compared to that of the RAE. Further, the averages are meaningful when they do not fluctuate with increasing size of the RAE.

By the application of divergence theorem and continuity conditions for displacements at the interfaces, it can be shown that

$$\bar{\varepsilon}_{ij} = \frac{1}{2hA}\int_C \int_{-h/2}^{h/2} \left(u_i n_j + u_j n_i\right) dz\, dC$$
$$\bar{\kappa}_{ij} = \frac{6}{h^3 A}\int_C \int_{-h/2}^{h/2} \left(u_i n_j + u_j n_i\right) z\, dz\, dC \qquad ; i,j = 1,2 \qquad (C2)$$
$$\bar{\gamma}_{i3} = \frac{1}{hA}\left[\int_C \int_{-h/2}^{h/2} u_3 n_i\, dz\, dC + \int_A \left\{u_i(h/2) - u_i(-h/2)\right\} dA\right]$$

where n_i, n_2 are the direction cosines of the normal at a point on the boundary C of the RAE.

Average in-plane stress resultants, moments and shear forces are defined as:

$$\overline{N}_{ij} = \frac{1}{A}\int_A \int_{-h/2}^{h/2} \sigma_{ij}\, dz\, dA$$

$$\overline{M}_{ij} = \frac{1}{A}\int_A \int_{-h/2}^{h/2} \sigma_{ij}\, z dz\, dA \qquad ; i,j = 1,2 \qquad (C3)$$

$$\overline{Q}_{ij} = \frac{1}{A}\int_A \int_{-h/2}^{h/2} \sigma_{i3}\, dz\, dA$$

By the use of the equilibrium equations, the divergence theorem and the continuity conditions for tractions across interfaces, the average stress resultants and moments can be related to the boundary tractions on the boundary C and top and bottom surfaces ($z = \pm h/2$) of the plate. These relations in symmetricized forms are given below:

$$\overline{N}_{ij} = \frac{1}{2A}\left[\int_C \int_{-h/2}^{h/2} \left(x_j T_i + x_i T_j\right) dz\, dC \right.$$
$$\left. + \int_A \left\{x_j\left[T_i(+h/2) + T_i(-h/2)\right] + x_i\left[T_j(+h/2) + T_j(-h/2)\right]\right\} dA \right]$$

$$\overline{M}_{ij} = \frac{1}{2A}\left[\int_C \int_{-h/2}^{h/2} \left\{\left(x_j T_i + x_i T_j\right)z - x_i x_j T_3\right\} dz\, dC \right. \qquad ; i,j = 1,2 \qquad (C4)$$
$$\int_A \left\{\frac{hx_j}{2}\left[T_i(+h/2) - T_i(-h/2)\right] + \frac{hx_i}{2}\left[T_j(+h/2) - T_j(-h/2)\right]\right.$$
$$\left.\left. - x_i x_j\left[T_3(+h/2) + T_3(-h/2)\right]\right]\right\} dA$$

$$\overline{Q}_i = \frac{1}{A}\left[\int_C \int_{-h/2}^{h/2} x_i T_3\, dz\, dC + \int_A x_i\left[T_3(+h/2) + T_3(-h/2)\right] dA\right.$$

It may be noted that when the surfaces $z = \pm h/2$ are stress free, the second integral over the area A on the right hand side of each of the above set of equations as zero and the average values $\overline{N}_{ij}, \overline{M}_{ij}$ and $\overline{Q}_i$ are expressed in terms of integrals evaluated over the boundary C. The same result is approached for sufficiently large RAE when the surface tractions are oscillatory and periodic functions of in-plane coordinates x_i, x_2. In addition, if

$$\int_C \int_{-h/2}^{h/2} x_i x_j T_3\, dz = 0 \qquad (C4a)$$

then $\overline{N}_{ij}, \overline{M}_{ij}$ are obtained from T_1 and T_2 on boundary C.

Constitutive Relations

For fabric reinforced plates containing repeating arrangement of weave patterns of the type shown in Figure C1, it is expected that the average stress resultants and moments will be re-

lated to the mid-plane strains and curvatures by constitutive relations similar to the ones used in laminated plate theory. For linear elastic problems, these relations are of the form given below.

$$\begin{bmatrix} \overline{N}_1 \\ \overline{N}_2 \\ \overline{N}_6 \\ \overline{M}_1 \\ \overline{M}_2 \\ \overline{M}_6 \end{bmatrix} = \begin{bmatrix} \overline{N}_{11} \\ \overline{N}_{22} \\ \overline{N}_{12} \\ \overline{M}_{11} \\ \overline{M}_{22} \\ \overline{M}_{12} \end{bmatrix} = \begin{bmatrix} A_{11}^* & A_{12}^* & A_{16}^* & B_{11}^* & B_{12}^* & B_{16}^* \\ A_{12}^* & A_{22}^* & A_{26}^* & B_{12}^* & B_{22}^* & B_{26}^* \\ A_{16}^* & A_{26}^* & A_{66}^* & B_{16}^* & B_{26}^* & B_{66}^* \\ & & & D_{11}^* & D_{12}^* & D_{16}^* \\ & \text{Sym.} & & D_{12}^* & D_{22}^* & D_{26}^* \\ & & & D_{16}^* & D_{26}^* & D_{66}^* \end{bmatrix} \begin{bmatrix} \overline{\varepsilon}_1 \\ \overline{\varepsilon}_2 \\ \overline{\varepsilon}_6 \\ \overline{\kappa}_1 \\ \overline{\kappa}_2 \\ \overline{\kappa}_6 \end{bmatrix} + \begin{bmatrix} \Gamma_1^* \\ \Gamma_2^* \\ \Gamma_6^* \\ \Delta_1^* \\ \Delta_2^* \\ \Delta_6^* \end{bmatrix} \qquad \text{(C5a)}$$

where $\begin{bmatrix} \overline{\varepsilon}_1 \\ \overline{\varepsilon}_2 \\ \overline{\varepsilon}_1 \\ \overline{\kappa}_1 \\ \overline{\kappa}_2 \\ \overline{\kappa}_6 \end{bmatrix} = \begin{bmatrix} \overline{\varepsilon}_{11} \\ \overline{\varepsilon}_{22} \\ 2\overline{\varepsilon}_{12} \\ \overline{\kappa}_{11} \\ \overline{\kappa}_{22} \\ 2\overline{\kappa}_{12} \end{bmatrix}$

and the last vector on the right hand side of (C5a) quantifies the stress resultants and moments due to change in temperature in absence of strains and curvatures. The relations (C5a) are obtained based on the following in-plane displacement fields

$$u_i = \left(\varepsilon_{ij} + z\kappa_{ij}\right)x_j \qquad \text{(C5b)}$$

and the interlaminar stress fields

$$\sigma_{zz} = \tau_{xz} = \tau_{yz} = 0 \qquad \text{(C5c)}$$

in each layer of the laminate, which yields

$$\left(A_{ij}^*, B_{ij}^*, D_{ij}^*\right) = \int_{-h/2}^{h/2} C_{ij}'\left(1, z, z^2\right) dz$$

$$\left(\Gamma_i^*, \Delta_i^*\right) = \int_{-h/2}^{h/2} \gamma_{ij}'(1, z, z)\, \Delta T\, dz \qquad ; \text{ i,j = 1,2,6} \qquad \text{(C5d)}$$

$$C_{ij}' = C_{ij} - C_{i3}C_{j3} / C_{33}$$

$$\gamma_i' = \gamma_i - C_{i3}\gamma_3 / C_{33}$$

where the constitutive law for each lamina is of the type

$$\sigma_i = C_{ij}\varepsilon_j + \gamma_i \Delta T \qquad ; \text{ i,j = 1,2, ...6} \qquad \text{(C5e)}$$

The strain energy in area A of the plate can be written in the following form in contracted notation

$$U = \frac{A}{2}\Big[A^*_{ij}\varepsilon_i\varepsilon_j + 2B^*_{ij}\varepsilon_i\kappa_j + D^*_{ij}\kappa_i\kappa_j + 2\left(\Gamma^*_i\varepsilon_i + \Delta^*_i\kappa_i\right) - F_T\Big] \qquad \text{(C5f)}$$

$$F_T = \int_{-h/2}^{h/2}\left(\left(\gamma_3\Delta T\right)^2 / C_{33}\right)dz$$

Midplane strains and curvature due to a temperature change alone are expressed in terms of thermal expansion and curvatures given by:

$$\begin{bmatrix}\alpha^*_1\\ \alpha^*_2\\ \alpha^*_6\\ \beta^*_1\\ \beta^*_2\\ \beta^*_6\end{bmatrix} = -\begin{bmatrix}A^* & B^*\\ B^* & D^*\end{bmatrix}^{-1}\begin{bmatrix}\Gamma^*_1\\ \Gamma^*_2\\ \Gamma^*_6\\ \Delta^*_1\\ \Delta^*_2\\ \Delta^*_6\end{bmatrix} \qquad \text{(C6)}$$

A^* and D^* matrices in equation (C5) and (C6) are the effective in-plane stiffnesses and bending rigidities and the B^* matrix contains the bending-extension coupling terms.

The shear forces are related to the average shear strains by relations of the following type

$$\begin{bmatrix}\overline{Q}_1\\ \overline{Q}_2\end{bmatrix} = \begin{bmatrix}K_{11} & K_{12}\\ K_{12} & K_{22}\end{bmatrix}\begin{bmatrix}\bar{\gamma}_{13}\\ \bar{\gamma}_{23}\end{bmatrix} \qquad \text{(C7)}$$

In subsequent stages of the work, we will study the effects of damages (crack like defect) and their growth due to increasing load. In such cases the elements of the matrices A^*, B^* and D^* may be assumed to depend on the state of strain in the RAE.

EVALUATION OF EFFECTIVE ELASTIC PROPERTIES

To evaluate the effective elastic properties, the standard technique is to first apply a homogeneous boundary condition in terms of displacements or tractions [C2] on the heterogeneous element (RAE). Sometimes it is advantageous to apply mixed conditions, i.e., some in terms of displacements and some in terms of tractions. If exact solutions can be found, then the strain or complementary energies in the element are equated to that in a homogeneous material to calculate the effective elastic properties. However, the geometric arrangements of the constituents are often so complicated that exact solutions are difficult to obtain and approximate solutions (simple or finite element calculations) are usually employed. In what follows we dis-

cuss some boundary conditions and give some approximate solutions which can yield bounds on effective properties as well as reasonable estimates of stress and strain fields in the RAE.

Boundary Conditions

We consider the following alternative types of boundary conditions on the surface S (consisting of C and $z = \pm h/2$) of the RAE. These choices are motivated by the displacement fields in a laminated plate due to prescribed midplane strains and/or curvatures.

Set 1

$$\begin{aligned} u_i &= \left(\varepsilon_{ij}^p + z\kappa_{ij}^p\right)x_j \qquad ;i = 1,2 \text{ on C} \\ T_3 &= 0 \qquad\qquad\qquad \text{on C} \\ T_1 &= T_2 = T_3 = 0 \qquad \text{on } z = \pm h/2 \end{aligned} \tag{C8a}$$

Set 2

$$\begin{aligned} u_i &= \left(\varepsilon_{ij}^p + z\kappa_{ij}^p\right)x_j \qquad ;i = 1,2 \\ T_3 &= 0 \qquad\qquad\qquad \text{on S} \end{aligned} \tag{C8b}$$

Set 3

$$\begin{aligned} u_i &= \left(\varepsilon_{ij}^p + z\kappa_{ij}^p\right)x_j \qquad ;i = 1,2 \\ u_3 &= -\frac{1}{2}\kappa_{ij}^p x_i x_j + F(z) \qquad \text{on S} \end{aligned} \tag{C8c}$$

where F(z) (constants at $z\pm h/2$ and a function z on C) is yet to be chosen. It may be noted that use of (C2) and the third of equation (C4) yields

$$\begin{aligned} \bar{\varepsilon}_{ij} &= \varepsilon_{ij}^p, \quad \bar{\kappa}_{ij} = \kappa_{ij}^p \\ \bar{Q}_{ij} &= 0 \end{aligned} \qquad \text{i,j - 1,2} \qquad \text{(C9a,b)}$$

for the boundary conditions (C8a) or (C8b), whereas for the case (C8c)

$$\begin{aligned} \bar{\varepsilon}_{ij} &= \bar{\varepsilon}_{ij}^p, \quad \bar{\kappa}_{ij} = \kappa_{ij}^p \\ \bar{\gamma}_{i3} &= 0 \end{aligned} \tag{C9c}$$

Therefore, they can be used to obtain the effective properties which relate the average stress resultants and moments to average midplane strains and curvatures.

For $\Delta T=0$, the strain energy in the RAE can be written in the following form

$$U^{\varepsilon} = \frac{1}{2}\int (T_1 u_1 + T_2 u_2 + T_3 u_3)\, dS \qquad \text{(C10)}$$

When $\Delta T \neq 0$, the following must be added to (C10)

$$U^{\Delta T} = \int \left(T_1^{\Delta T} u_1 + T_2^{\Delta T} u_2 + T_3^{\Delta T} u_3\right) dS \qquad \text{(C11)}$$

The integrals in (C10) and (C11) are evaluated on surfaces where the tractions are not prescribed as zero (as in (C8a) or (C8b)). Using (C8a-c), (C4), (C10) and (C11) one obtains

$$U^{\varepsilon} = \frac{A}{2}\left[\overline{N}_{ij}\varepsilon_{ij}^{p} + \overline{M}_{ij}\kappa_{ij}^{p} + C_1\right] \qquad \text{for } \Delta T=0 \qquad \text{(C12a)}$$

$$U^{\Delta T} = A\left[\overline{N}_{ij}^{\Delta T}\varepsilon_{ij}^{p} + \overline{M}_{ij}^{\Delta T}\kappa_{ij}^{p} + C_1^{\Delta T}\right] \qquad \text{for } \Delta T\neq 0 \qquad \text{(C12b)}$$

where

$$C_1 = 0 \qquad \text{for cases (C8a,b)} \qquad \text{(C13a)}$$

$$C_1 = \int_A \int_{-h/2}^{h/2} F'(z)\sigma_{33}\, dz\, dA / A \qquad \text{for case (C8c)} \qquad \text{(C13b)}$$

$\overline{N}_{ij}$, $\overline{M}_{ij}$ are related to the tractions by (C4). The quantities with superscript ΔT are due to temperature change alone. If the woven or fabric reinforced plate has a constitutive law similar to (C5), then (C12) and (C13) indicates that the strain energy is of a form similar to (C5f). It may be noted that the term C_1 or $C_1^{\Delta T}$ for case (C8c) appear because of the integral $\int T_3 F(z) ds$ and $T_3 \neq 0$ in this case. The last of (C13) is obtained by the use of the divergence theorem and the equilibrium equation in terms of stresses (in z-direction) in the following manner

$$\int T_3 u_3\, dS = \int_{C-h/2}^{h/2} \int T_3 F(z)\, dz\, dC + \int_A \left(T_3(h/2)F(h/2) + T_3(-h/2)F(-h/2)\right) dA \qquad \text{(C14a)}$$

and

$$\begin{aligned} \int\int T_3 F(z)\, dC\, dz &= \int\int \tau_{3i}\upsilon_3 F(z)\, dC\, dz \\ &= \int\int \tau_{3i,i} F(z)\, dz\, dA \\ &= -\int\int \sigma_{33.,3} F(z)\, dz\, dA \qquad \text{(C14b)} \\ = -\int_A (T_3(h/2)F(h/2) + T_3(-h/2)F(-h/2))dA &+ \int_A \int_{-h/2}^{h/2} F'(z)\sigma_{33}\, dz\, dA \end{aligned}$$

The first term on the last expression of (C14b) cancels with the second term in (C14a) and we obtain the expression C_1 as it appears in (C13b).

A Simple Upper Bound

For a displacement field, we assume that equation (C8c) also holds inside the RAE and F(z) is yet an unknown function of z and its derivative is

$$f(z) = dF(z)/dz \tag{C15}$$

It follows, therefore, that the state of strain in the RAE is given by

$$\begin{aligned} &\varepsilon_{ij} = \varepsilon_{ij}^{p} + z\kappa_{ij}^{p} \qquad ; i,j = 1,2 \\ &\varepsilon_{33} = f(z) \\ &\text{and} \\ &\gamma_{i3} = 0 \qquad ; i = 1,2 \end{aligned} \tag{C16}$$

and the total potential energy for the assumed field can be written in the following form using the contracted notation

$$\begin{aligned} U^{\varepsilon} = \frac{1}{2}\int_{A}\int_{-h/2}^{h/2} \Big[& C_{ij}\left(\varepsilon_i^p\varepsilon_j^p + 2z\varepsilon_i^p\kappa_j^p + \kappa_i^p\kappa_j^p\right) \\ & + C_{33}f^2(z) + 2C_{i3}\left(\varepsilon_i^p + z\kappa_i^p\right)f(z) \\ & + \left\{2\gamma_i(\varepsilon_i^p + z\kappa_i^p) + 2\gamma_3 f(z)\right\}\Delta T\Big]dz\,dA \end{aligned} \tag{C17}$$

where the C_{ij} and γ_I, are the thermoelastic constants which are functions of position and their values depend on the constituent r with the following constitutive law (similar to C5f)

$$\sigma_i = C_{ij}\varepsilon_j + \gamma_i\Delta T \qquad i,j = 1,2,3,6 \tag{C18}$$

It may be noted that for a laminated plate, equation (C17) reduces to the energy expression as per the laminated plate theory solution provided f(z) is in each lamina is chosen so as to make $\sigma_{33} = 0$ in that lamina for the strain state (C16). For the plate with a woven construction, we note that

$$U^{\varepsilon} \geq U \tag{C18}$$

where U^{ε} is given by (C17) and U is the actual strain energy (or potential energy) which must be a minimum. We can now write (C17) as

$$\begin{aligned} U^{\varepsilon} = \frac{A}{2}\int_{-h/2}^{h/2} \Big[& C_{ij}^{a}\left(\varepsilon_i^p + z\kappa_i^p\right)\left(\varepsilon_j^p + z\kappa_j^p\right) \\ & + C_{33}^{a}f^2(z) + 2C_{i3}^{a}\left(\varepsilon_i + z\kappa_i^p\right)f(z) \\ & + 2\gamma_i^{a}\left(\varepsilon_i^p + z\kappa_i^p\right) + 2\gamma_3^{a}f(z)\Big]dz \end{aligned} \tag{C19}$$

where

$$c_{ij}^{a} = \int_{A} C_{ij}\, d\,A / A$$
$$\gamma_{i}^{a} = \int_{A} \gamma_{i}\Delta T\, d\,A / A \qquad \text{(C20)}$$

We may now seek a minimum value of U^{ε} for determining f(z) which yields

$$f(z) = -\frac{C_{i3}^{a}\left(\varepsilon_{i}^{p} + z\kappa_{i}^{p}\right) + \gamma_{3}^{a}}{C_{33}^{a}} \qquad \text{(C21)}$$

which also implies that

$$\int \sigma_{33} dA = 0 \qquad \text{for all z} \qquad \text{(C22)}$$

and therefore from (C13)

$$C_{1} = C_{1}^{\Delta T} = 0$$

for case C8c.

Substitution of (C21) in (C19) yields the following expression for U^{ε}

$$U^{\varepsilon} = \frac{A}{2}\Big[\left(A_{ij}^{1}\varepsilon_{i}^{p}\varepsilon_{j}^{p} + 2B_{ij}^{1}\varepsilon_{i}^{p}\kappa_{j}^{p} + D_{ij}^{1}\kappa_{i}^{p}\kappa_{j}^{p}\right.$$
$$\left. + 2\left(\Gamma_{i}^{1}\varepsilon_{i}^{p} + \Delta_{i}^{1}\kappa_{i}^{p}\right) - F_{T}^{1}\ \right] \qquad \text{(C23)}$$

where

$$\left(A_{ij}^{1}, B_{ij}^{1}, D_{ij}^{1}\right) = \int_{-h/2}^{h/2} C_{ij}^{1'}(1, z, z^{2})dz$$
$$\left(\Gamma_{i}^{1}, \Delta_{i}^{1}\right) = \int_{-h/2}^{h/2} \gamma_{i}^{1'}(1, z)dz$$
$$C_{ij}^{1'} = C_{ij}^{a} - C_{i3}^{a}C_{j3}^{a} / C_{33}^{a} \qquad ;\ i,j = 1,2,6 \qquad \text{(C26)}$$
$$\gamma_{i}^{1'} = \gamma_{i}^{a} - C_{i3}^{a}\gamma_{3}^{a} / C_{33}^{a}$$

and

$$F_{T}^{1} = \int_{-h/2}^{h/2}\left(\left(\gamma_{3}^{a}\right)^{2} / C_{33}^{a}\right)dz$$

These results yield upper bound type estimates of the desired effective thermoelastic constants for the plate and they can be evaluated for any known geometric arrangement obtained by stacking fabric reinforced layers with or without stitching or other through the thickness reinforcements. It may be noted that for the case when several fabric reinforced layers are stacked up, it is only necessary to evaluate the effective constants for one layer and then using the following relations to compute the properties for the plate.

$$[A] = \sum_k \left[A^{lk}\right]$$

$$[B] = \sum_k \left[A^{lk}\right] z_o^k + \left[B^{lk}\right]$$

$$[D] = \sum_k \left[A^{lk}\right] (z_o^k)^2 + 2\left[B^{lk}\right] z_o^k + \left[D^{lk}\right]$$

Where the summation is taken over all layers (denoted with superscript k) and z_o^k is the distance of the midplane of the layer k from the midplane of the plate. It may be noted that the results given above also yield upper bound estimates for the whole plate since the displacement compatibility is satisfied everywhere. These results can be viewed as a generalization of results obtained for effective moduli of fabric layers based on the assumption of iso-strain conditions [C1].

More accurate upper bound estimates can be obtained by choosing other types of displacement fields in the RAE subjected to boundary conditions (C8a), (C8b), or (C8c). Condition (C8a) imposes less restrictive conditions on displacements and, therefore, may be better suited to allow simple choices of other fields. However, since the geometry is usually quite complicated, it may be necessary to obtain numerical solutions for nonzero value of one prescribed quantity such as ε_1^p and zero values for others and evaluate the total strain energy in all the constituent regions (or by evaluating $\overline{N}_{ij}$ and $\overline{M}_{ij}$ by using (C4)).

REFERENCES

C1. Cox, B.N. and Flanagan, G., Handbook of Analytical Methods of Textile Composites, Version 1.0, Rockwell Aerospace, NASA Contractor Report, NAS1-19243, May 1996.

C2. Hashin, Z., Theory of Fiber Reinforced Composites, NASA CR-1974, March 1972.

APPENDIX D

USE OF P-ELEMENTS FOR STRESS ANALYSIS OF A TEXTILE

Suite 250, 500 Office Center Drive
Fort Washington, PA 19034
Tel: 215-542-8400 Fax: 215-542-8401

APPENDIX D USE OF P-ELEMENTS FOR STRESS ANALYSIS OF A TEXTILE

INTRODUCTION AND SUMMARY

Additional innovative analysis approaches were also investigated. One approach was to use P-element technology to model textiles. P-elements use increasing polynomial order to obtain convergence. A major advantage of the approach is that single elements can be used to represent large portions of the textile architecture, potentially simplifying the modeling. A commercial P-element code called Mechanica [D1] was used to test the approach. This provides a high resolution picture of the linear stresses within the textile unit-cell. However, the modeling tools available in the commercial package, while more expedient than tradition FE meshing methods, were too time consuming, and are difficult to automate. This drawback, combined with the limitation that the P-element method cannot handle general nonlinear material properties has lead us to focus on tradition FE methods.

DISCUSSION

The P-element model is based on the same geometric assumptions used in the automated meshing routines described above. The geometry was transferred to Mechanica as a series of curves, and the mesh created using the graphical tools provided in the software. Figures D1 and D2 show portions of the resulting model. The individual P-elements can form into the shape of the undulating section, allowing for a comparatively coarse mesh. General repeating boundary conditions are not possible in this code (due to the lack of a mult-point constraint capability). By using symmetry conditions, the axial load condition can be applied.

Stress results for a segment of warp yarn are shown in Figures D4-D6, using the coordinate system shown in Figure D3. The results are for a fixed displacement in the warp direction, resulting in an average σ_{11} stress of 22.9 GPa. These figures show how the undulations give rise to σ_{33}, and τ_{13} stresses which can cause intra-bundle cracking. In addition, there is a concentration of σ_{11} stress that will reduce the fiber failure loads as compared to a conventional laminate. The maximum stresses in a warp yarn, normalized by the unit cell average stress, are summarized in Table D1.

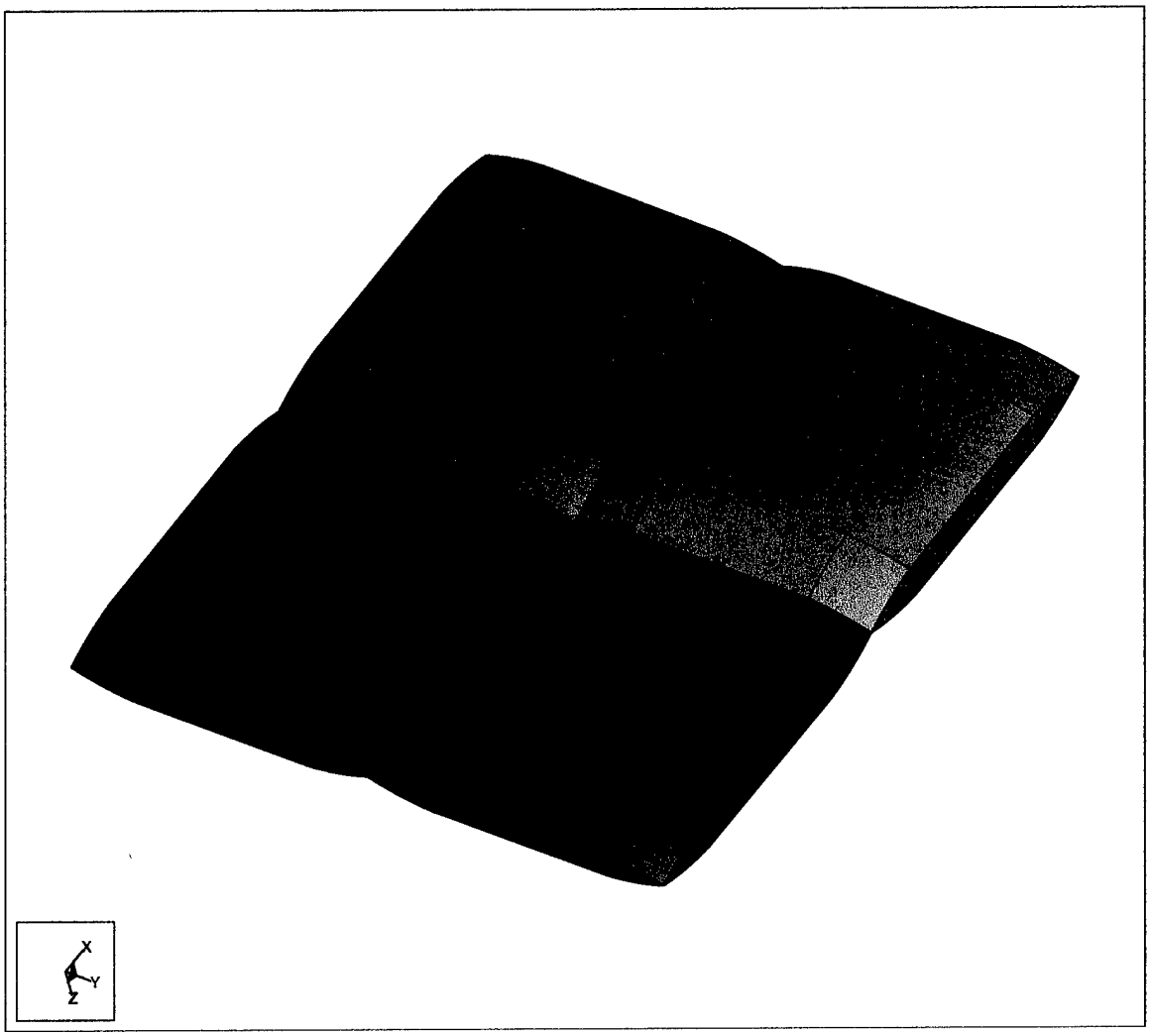

Figure D1. P-Element Model of Yarns for Plain-Weave Unit Cell

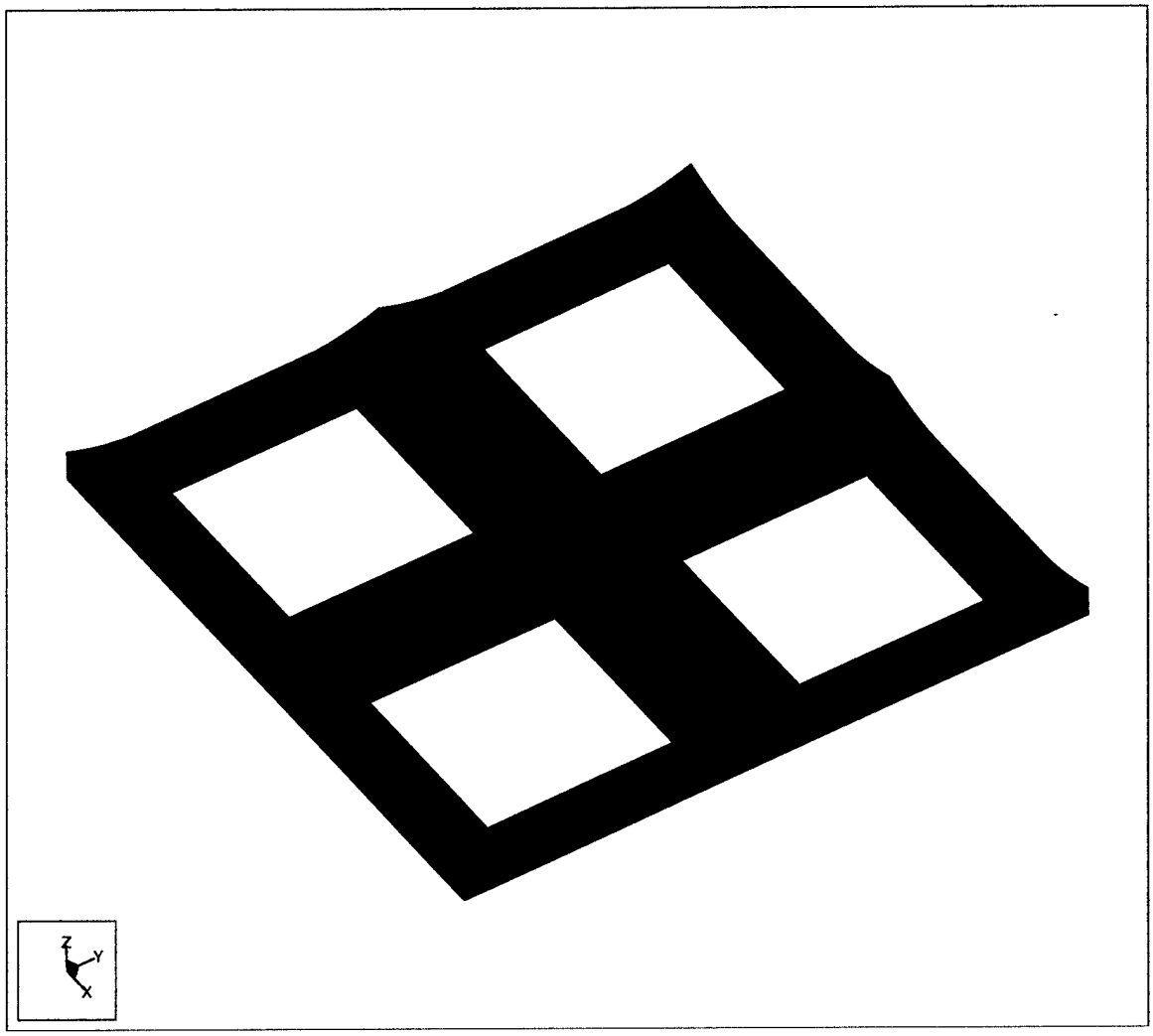

Figure D2. P-Element Model of Matrix Pockets for Plain-Weave Unit Cell

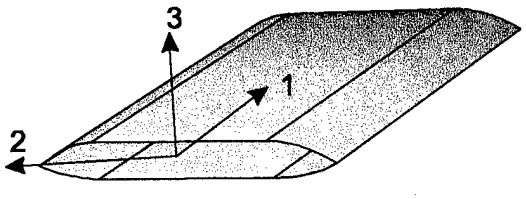

Figure D3. Local Yarn Coordinate System for Stress Results

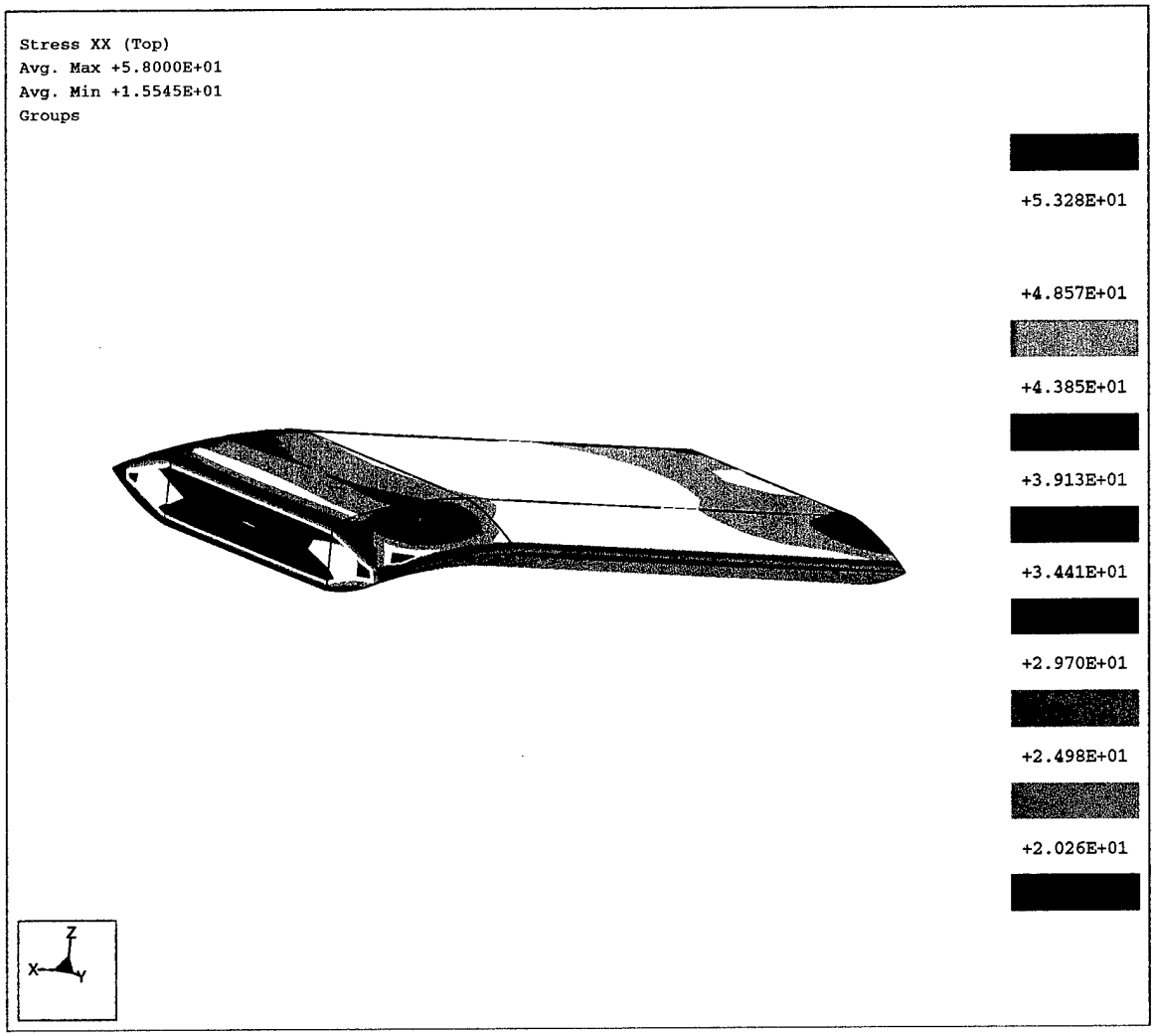

Figure D4 Fiber Direction Stress (σ_{11}) in Segment of Warp Yarn. Textile Loaded in Warp Direction with Average Stress of σ_{11}^{0}=22.9 GPa

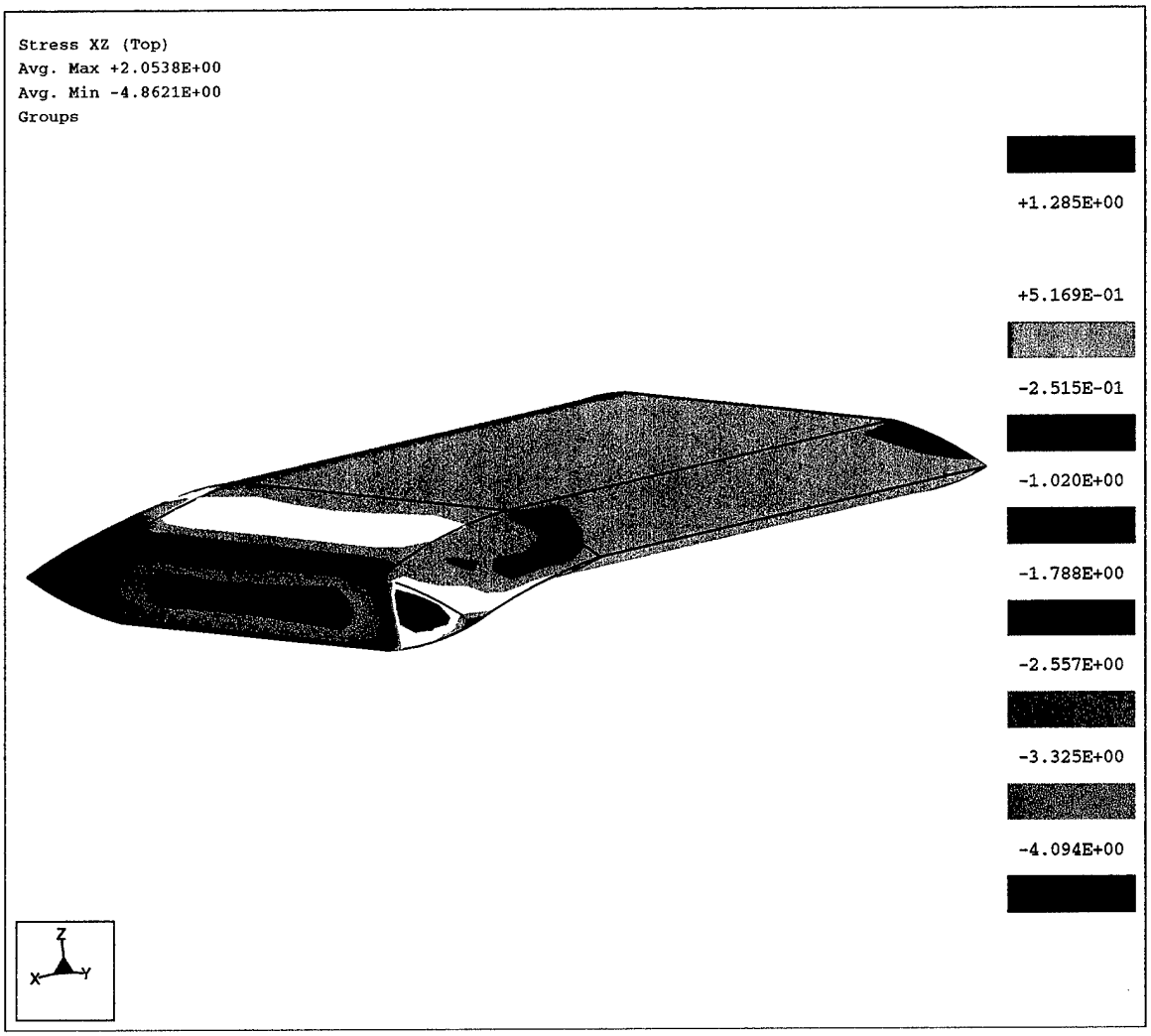

Figure D5 Interlaminar Shear Stress (τ_{13}) in Segment of Warp Yarn. Textile Loaded in Warp Direction with Average Stress of σ_{11}^{0}=22.9 GPa

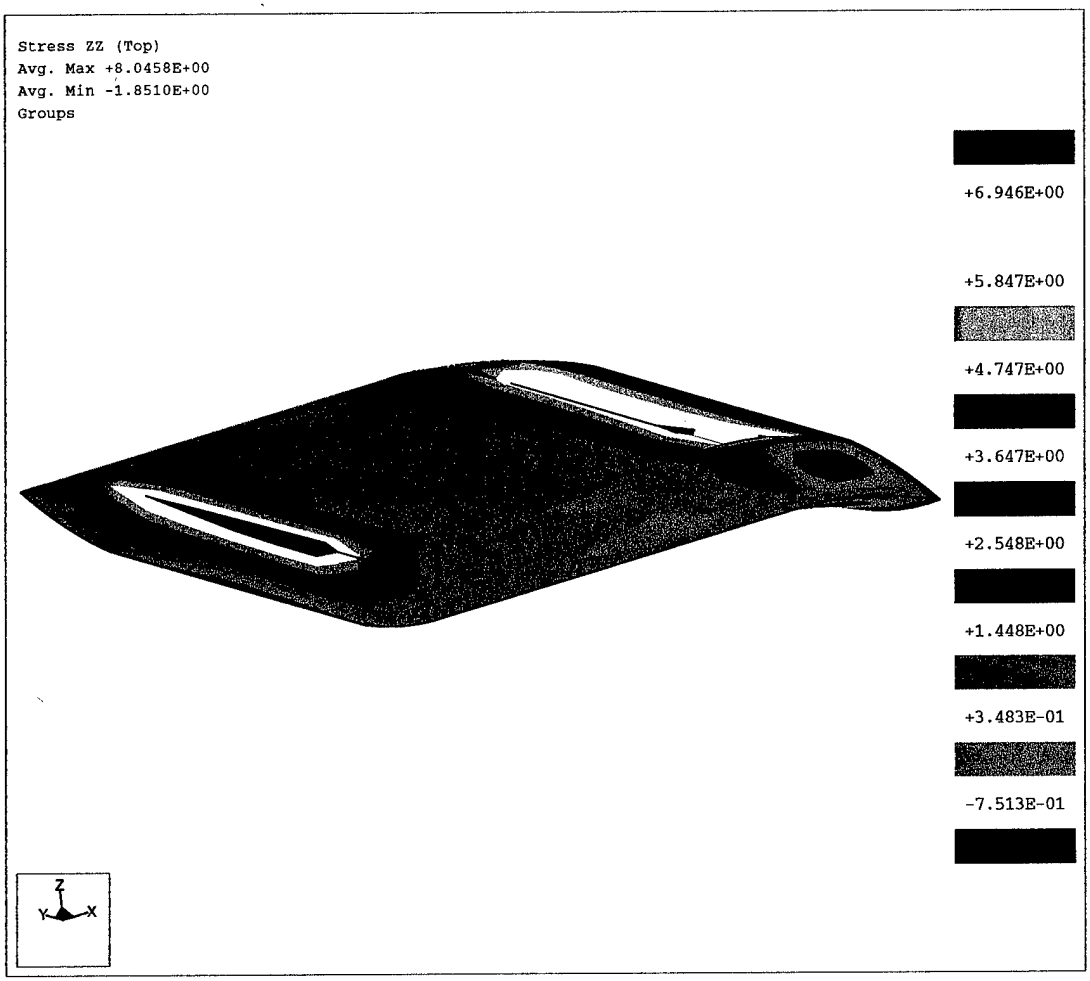

Figure D6 Vertical Stress (σ_{33}) in Segment of Warp Yarn. Textile Loaded in Warp Direction with Average Stress of σ_{11}^{0}=22.9 GPa

Table D1 Ratios of Maximum Stress Components to Average Applied Warp Direction Stress

Component	Ratio
$\sigma_{11}^{max}/\sigma_{11}^{0}$	2.52
$\sigma_{13}^{max}/\sigma_{11}^{0}$	0.212
$\sigma_{33}^{max}/\sigma_{11}^{0}$	0.350

REFERENCES

D1. Pro/MECHANICA, Release 17.0 (1996), Parametric Technology Corporation, Waltham, MA.